

Chapter 2

A New Approach to the Understanding of the Mechanism of Lead Electrodeposition

Nebojša D. Nikolić and Konstantin I. Popov

2.1 Introduction

The most important applications of lead include the production of high purity active materials for acid battery [1], for semiconductors [2, 3], and for the fabrication of electrochromic devices [4]. In the form of powder, lead is widely used in industries of gas and oil exploration, radiological medical protective clothing, as an industrial X-ray shield, golf club manufacture, and antifriction products [5]. The electrodeposition technique is a very suitable way to obtain lead in the form suitable for the application in the above-mentioned technologies. For example, the advantage of use of electrodeposition technique in the production of lead in the powder form lies in the fact that lead powder is produced at low overpotentials and hence with small spent of energy. The open porous structures of lead with the extremely high surface area (the honeycomb-like ones), which are ideally situated for electrodes in electrochemical devices such as fuel cells, batteries, and sensors, are also possible to get by the electrodeposition techniques [6].

Aside from the practical significance, the processes of lead electrodeposition also have the high scientific significance in the examination of the fast electrochemical processes. In the Winand's classification of metals [7], Pb belongs to the group of normal metals together with Ag, Cd, Zn, and Sn. These metals are characterized by low melting points and high exchange current densities, j_0 .

N.D. Nikolić (✉)

ICTM-Institute of Electrochemistry, University of Belgrade, Njegoševa 12,
11001 Belgrade, Serbia

e-mail: nnikolic@tmf.bg.ac.rs

K.I. Popov

ICTM-Institute of Electrochemistry, University of Belgrade, Njegoševa 12,
11001 Belgrade, Serbia

Faculty of Technology and Metallurgy, University of Belgrade, Karnegijeva 4,
11001 Belgrade, Serbia

e-mail: kosta@tmf.bg.ac.rs

For lead electrodeposition, both alkaline [8, 9] and acidic [4, 10–22] electrolytes are widely used. The most often employed acidic electrolytes are those based on chloride [10, 11], bromide [12], iodide [12], nitrate [4, 13, 14], fluoroborate [15], acetate [16], fluorosilicate [17–20], methanesulfonate [21, 22], etc.

Depending on the type and composition of the electrolyte and electrodeposition conditions, various powders, e.g. dendritic [16], honeycomb-like structures [6], etc. can be obtained. On the other hand, smooth, adherent, and compact deposits can be formed in the presence of additives such as phenol, ethanol, gelatin [23], sodium lignin sulfonate, chestnut extract, and animal glue [17–20]. Furthermore, the additions of sorbitol [24] and glycerol [8] to the electroplating solutions have some effect on the morphology of the electrodeposited lead.

It is believed that the electrodeposition processes of normal metals are diffusion controlled. However, it was shown recently [25–29] that the linear dependence of the current density on the overpotential during silver electrodeposition from nitrate solution could be ascribed to an ohmic controlled electrodeposition process. Regarding the affiliation to the same group of metals, the well-defined linear dependence of the current density on overpotential during lead electrodeposition from a concentrated nitrate solution was also observed [30, 31]. The new investigations of the mechanism of lead electrodeposition showed that electrodeposition of this metal can follow the mixed ohmic-diffusion control [32]. For that reason, the aim of this chapter was a comprehensive survey of all aspects related with the processes of lead electrodeposition.

2.2 Mechanism of Lead Electrodeposition: The Mixed Ohmic-Diffusion and the Full Ohmic Control

2.2.1 Polarization Characteristics: Experimental Evidence

Figure 2.1 shows the polarization curves for lead electrodeposition from solutions containing 0.050, 0.10, 0.20 (Fig. 2.1a), and 0.30 and 0.45 M $\text{Pb}(\text{NO}_3)_2$ (Fig. 2.1b) in 2.0 M NaNO_3 . The following experimental procedure, usual for the recording of the polarization curves of fast electrochemical processes, was applied to obtain a reproducible shape of the polarization curves for lead [32]: the values of the current density obtained after stabilization of their values at every 5 mV were used for constructing the polarization curves. The time required for stabilization of the current density values was 3 s at all overpotentials. After the determined values of overpotential (the inflection point), the current density increased dramatically and then the values of the current density at the moment selected values of the overpotential were attained were employed for the further recording of the polarization curves.

The common characteristic of all the polarization curves is the existence of an inflection point at an overpotential of 55 mV, followed by a sharp increase in the

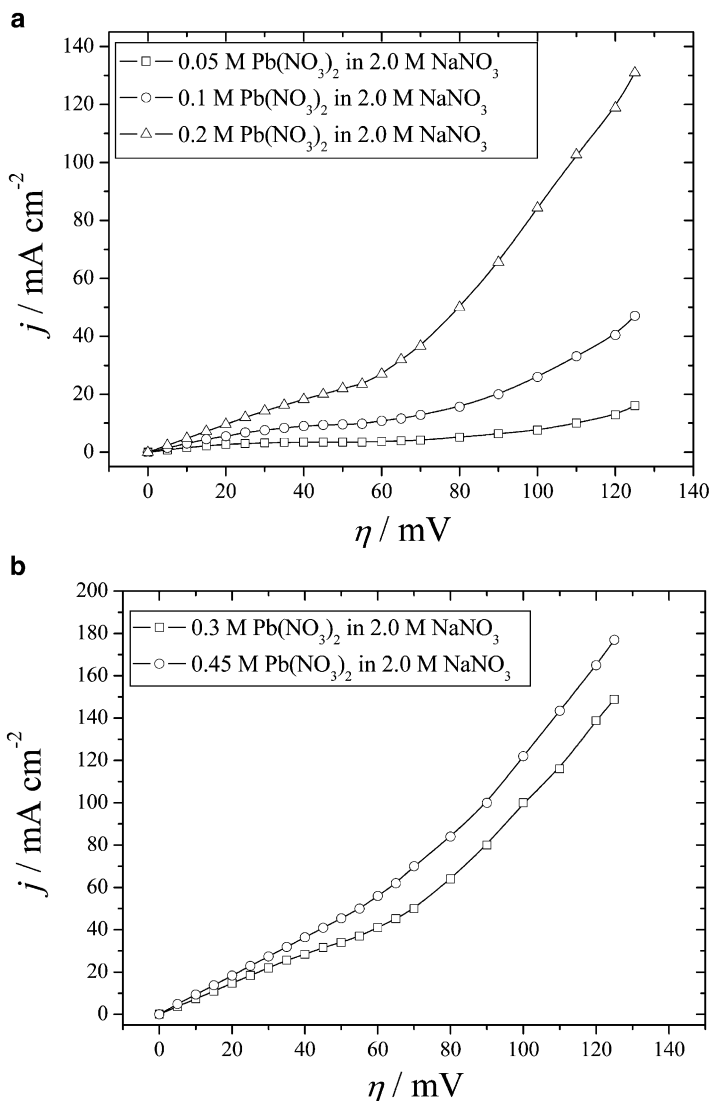


Fig. 2.1 Polarization curves for lead electrodeposition from: (a) 0.050, 0.10, 0.20 and (b) 0.30 and 0.45 M $\text{Pb(NO}_3)_2$ in 2.0 M NaNO_3 (Reprinted from [32] with permission from Elsevier.)

current density on further increasing the overpotential. A careful analysis of the parts of polarization curves up to an overpotential of 55 mV (Fig. 2.2) showed that the polarization curves recorded from solutions containing 0.050, 0.10, 0.20, and 0.30 M $\text{Pb(NO}_3)_2$ in 2.0 M NaNO_3 consisted of two parts: (a) linear dependencies of the current density on overpotential, which were ascribed to ohmic controlled electrodeposition and (b) the parts corresponding to diffusion controlled

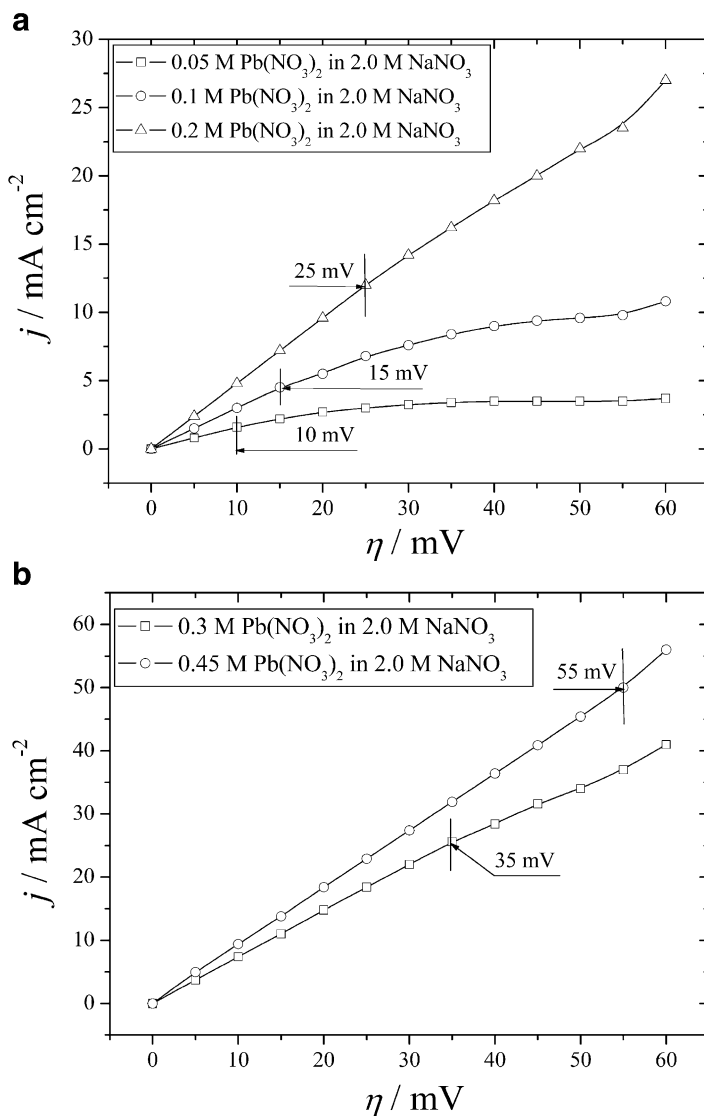


Fig. 2.2 The parts of the polarization curves up to an overpotential of 55 mV: (a) 0.050, 0.10, 0.20 and (b) 0.30 and 0.45 M $\text{Pb}(\text{NO}_3)_2$ in 2.0 M NaNO_3 (Reprinted from [32] with permission from Elsevier.)

electrodeposition. A well-defined plateau of the limiting diffusion current density could be noticed on the polarization curve recorded from the solution of the lowest analyzed $\text{Pb}(\text{II})$ concentration (0.050 M $\text{Pb}(\text{NO}_3)_2$ in 2.0 M NaNO_3). For this solution, the linear dependence of the current density on overpotential (ohmic control of electrodeposition) was in the interval of overpotentials from 0 to 10 mV.

The length of this linear dependence increased with increasing concentration of Pb (II) ions. Simultaneously, the region of diffusion control of the electrodeposition decreased, while the slope of the inclined limiting diffusion current density plateau increased. The values of the overpotentials corresponding to the end of the ohmic control of the electrodeposition process are denoted in Fig. 2.2 by a vertical line. Nevertheless, these curves can be denoted as typical representatives of mixed ohmic-diffusion control of the electrodeposition process.

The plateaus of the limiting diffusion current density vanish with further increase of the Pb(II) ions concentration, becoming an inflection point at an overpotential of 55 mV (0.45 M Pb(NO₃)₂ in 2.0 M NaNO₃—Fig. 2.1b). A linear dependence of the current density on overpotential was observed up to the inflection point. This polarization curve represents a typical example of complete ohmic control of the electrodeposition process. A similar shape of the polarization curve was previously recorded from 0.50 M Pb(NO₃)₂ in 2.0 M NaNO₃ [30, 31], as well as in the case of electrodeposition of some other metals from this group, such as silver [25–29]. A sharp increase in the current density with increasing overpotential after the inflection point was also observed.

2.2.2 General Discussion of the Mechanism of Lead Electrodeposition

Electrodeposition of lead occurred under conditions of natural convection, which results in a linear dependence of the logarithm of the limiting diffusion current density on the logarithm of the concentration of the depositing ions.

Namely, the mass and heat transfer induced by the density gradient in liquids in the gravitational field is natural or free convection [25, 33, 34]. Levich [33] gave an approximate analytical solution for the estimation the diffusion flux of the component that reacts and disappears on the surface of a vertical plate in a liquid. The electrodeposition of metals is a fair example of this kind of reaction [25].

According to Levich, in non-stirred electrolytes under conditions of natural convection, the limiting diffusion current density, j_L , varies with concentration of solution, c , as

$$j_L \approx c^n, \quad (2.1)$$

where:

$$1 \leq n \leq 1.25. \quad (2.2)$$

When the temperatures of the thermostated solutions (with a free surface) and of the surrounding air are the same, $n = 1.25$ and this value corresponds to proper isothermal conditions [34]. The values $n \leq 1.25$ correspond to non-isothermal conditions, i.e., when there are differences between these temperatures.

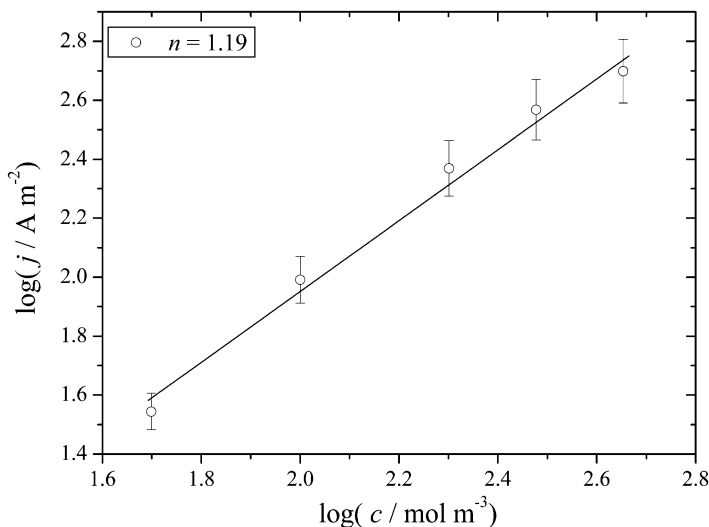
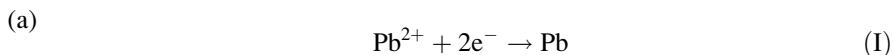


Fig. 2.3 The logarithmic dependence of the limiting diffusion current density, j_L , on the concentration of solution, c . The values of the limiting diffusion current density correspond to the inflection points on the polarization curves ($\eta = 55$ mV) (Reprinted from [32] with permission from Elsevier.)

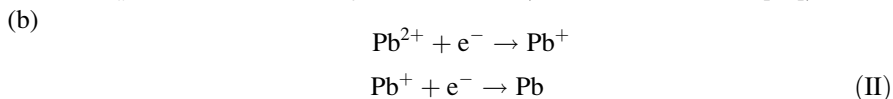
The logarithmic dependence of j_L on c is shown in Fig. 2.3, and the slope n was found to be 1.19. It is necessary to stress that the current densities corresponding to the inflection points on the polarization curves, i.e., an overpotential of 55 mV, were taken as the limiting ones. The excellent agreement between theoretical prediction and the experimentally obtained value confirmed that the electrodeposition of lead occurs under conditions of natural convection.

The polarization curves (Fig. 2.2) standardized to the values of the limiting diffusion current density are given in Fig. 2.4. An analysis of Fig. 2.4 clearly indicated that the ratio of the ohmic control to the overall control of electrodeposition process increased with increasing concentration of Pb(II) ions.

There is no evidence about the true reaction mechanism for lead electrodeposition, but two reaction mechanisms are possible:



with $b_a = 60$ mV/dec and $b_c = 60$ mV/dec (the case of cadmium [35]), and



with $b_a = 40$ mV/dec and $b_c = 120$ mV/dec (the case of copper [36]).

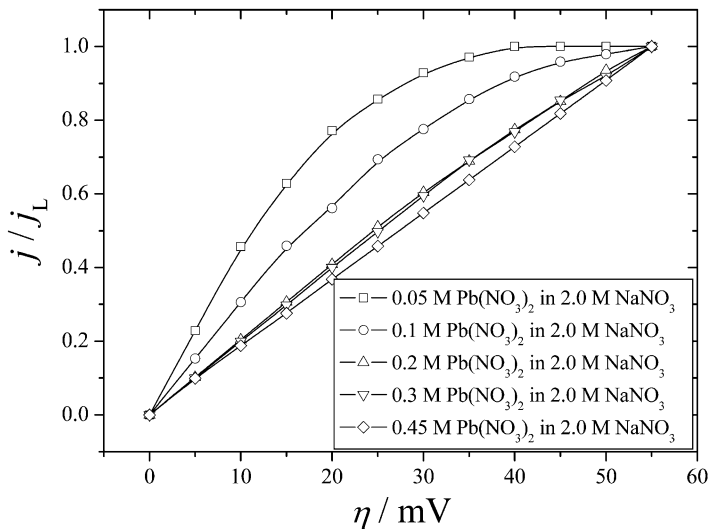


Fig. 2.4 The polarization curves standardized to the values of the limiting diffusion current density (Reprinted from [32] with permission from Elsevier.)

Although the reaction mechanism (I) is more probable than mechanism (II), we are of the opinion that reaction mechanism (II) should not be completely disregarded [32].

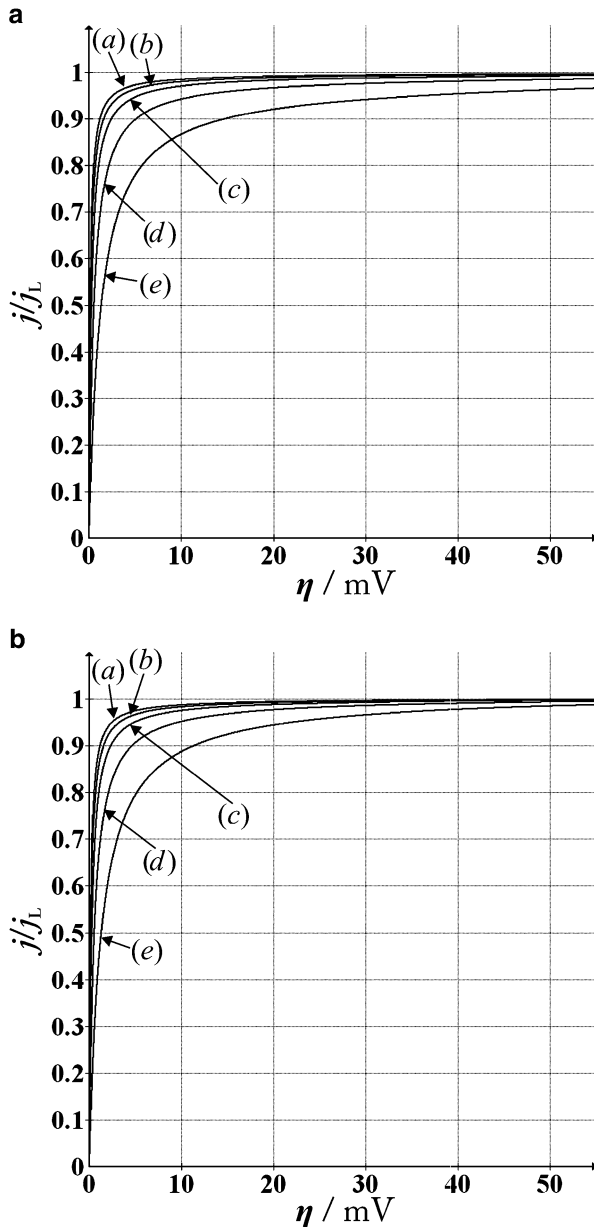
For the very fast electrodeposition reactions, the following form of the polarization curve equation is valid [27, 28]:

$$j = \frac{j_0(f_c - f_a)}{1 + \frac{j_0}{j_L}(f_c - f_a)}. \quad (2.3)$$

In Eq. (2.3), $f_c = 10^{\eta/bc}$, $f_a = 10^{-\eta/ba}$, j is the current density, and η is the overpotential (the cathodic current density, j and η are taken as positive values).

Figure 2.5 shows the dependencies of j/j_L on η for the different j_0/j_L ratios [(a)— $j_0/j_L = 100$, (b)— $j_0/j_L = 75$, (c)— $j_0/j_L = 50$, (d)— $j_0/j_L = 25$, and (e)— $j_0/j_L = 10$] obtained by the simulation of Eq. (2.3) for the two possible mechanisms of lead deposition: (a) (I)—Fig. 2.5a and (b) (II)—Fig. 2.5b. Both dependencies are practically the same when $j_0/j_L \geq 10$, indicating that there is no effect of the different Tafel slopes on the shape of the polarization curves. This is better illustrated in Fig. 2.6, which shows a comparative survey of the dependencies of j/j_L on η for the j_0/j_L ratios of 100, 50, and 10 for the both reaction mechanisms. From Fig. 2.5, it can also be seen that for $j_0/j_L \geq 50$, the systems enter full diffusion control at $\eta > 10$ mV, being under complete ohmic control up to $j \approx 0.9j_L$. Moreover, differences in the polarization characteristics of lead between these two reaction mechanisms are not expected due to the absence of activation control of the electrodeposition. The dependencies shown in Figs. 2.5 and 2.6 were calculated without inclusion of an ohmic potential

Fig. 2.5 The dependencies of j/j_L on η for the different j_0/j_L ratios obtained by the simulation of Eq. (2.3) for the possible lead reaction mechanisms: (a) (I) and (b) (II). The markings in the figure: (a) $j_0/j_L = 100$, (b) $j_0/j_L = 75$, (c) $j_0/j_L = 50$, (d) $j_0/j_L = 25$, and (e) $j_0/j_L = 10$ (Reprinted from [32] with permission from Elsevier.)



drop in the overpotential. On the other hand, an ohmic potential drop is included in the experimentally obtained polarization curves (Fig. 2.4). This means that a comparison of the calculated and experimentally obtained polarization curves is impossible without elimination of the ohmic potential drop from the experimentally obtained polarization curves.

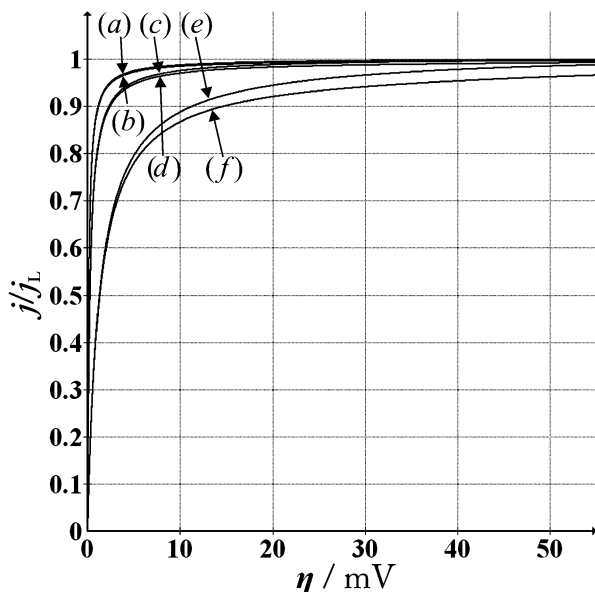


Fig. 2.6 The comparative survey of the dependencies of j/j_L on η for the different j_0/j_L ratios obtained for the both groups of Tafel slopes. The markings in the figure: (a), (c), and (e)—Reaction mechanism: (I), and (b), (d), and (f)—Reaction mechanism: (II), (a) and (b) $j_0/j_L = 100$; (c) and (d) $j_0/j_L = 50$; (e) and (f) $j_0/j_L = 10$ (Reprinted from [32] with permission from Elsevier.)

The recently proposed procedure [25] was used for the elimination of the ohmic potential drop from the experimentally obtained polarization curves. This procedure can be presented briefly as follows: at a specified current density, the difference between the experimentally measured overpotential and the one corresponding to full ohmic control of the electrodeposition is the diffusion overpotential, η_{diff} . Naturally, the above consideration is only valid before the abrupt increase in the current density with the increasing overpotential after the inflection point. This way of correction for the ohmic potential drop is illustrated in Fig. 2.7a for the part of the polarization curve up to the inflection point recorded from the solution containing 0.050 M $\text{Pb}(\text{NO}_3)_2$ in 2.0 M NaNO_3 . In this way, corrected polarization curves, shown in Fig. 2.7b, suitable for discussion of the initiation of dendritic growth were obtained. It is necessary to remember that the corrected values of the overpotentials represent only diffusion ones, η_{diff} .

Hence, it could be concluded from Fig. 2.7b that in mixed ohmic-diffusion control of the electrodeposition (the systems with $j_0 \gg j_L$), increasing concentration of $\text{Pb}(\text{II})$ ions causes a decrease in both the critical overpotential for dendritic growth initiation, η_i , and the critical overpotential for instantaneous dendritic growth, η_c . A qualitative comparison with the simulated dependencies shown in Fig. 2.5 was thus enabled by standardization of the current density values from Fig. 2.7b to the corresponding limiting diffusion current density values.

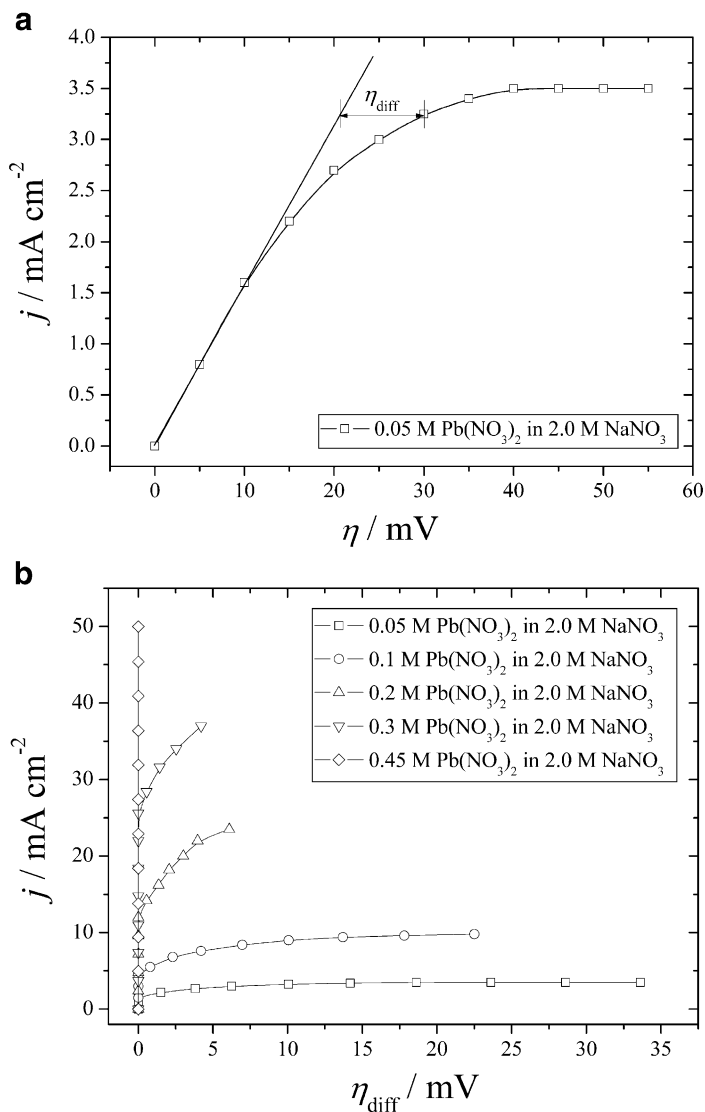


Fig. 2.7 (a) The way of the correction of the ohmic potential drop in the experimentally obtained polarization curves and (b) the corrected parts of polarization curves up to the inflection point j on η_{diff} (Reprinted from [32] with permission from Elsevier.)

The standardized dependencies $j/j_L - \eta_{\text{diff}}$ are shown in Fig. 2.8. Based on the dependencies shown in Figs. 2.5 and 2.8, it is very clear that increasing the concentration of Pb(II) ions leads to a strong increase in the j_0/j_L ratio.

This situation is completely different from the one observed in the activation–diffusion controlled electrodeposition (the systems characterized by $j_0 < j_L$; e.g., copper). In the activation–diffusion control of electrodeposition process, both η_i and

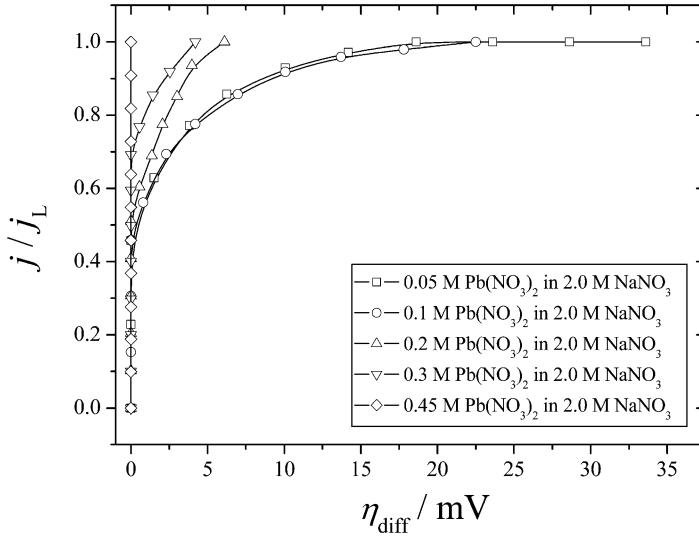


Fig. 2.8 The standardized dependencies of j/j_L on η_{diff} (Reprinted from [32] with permission from Elsevier.)

η_c increased with increasing concentration of the depositing ions, indicating a decrease of the j_0/j_L ratios with the increasing concentration of metal ions.

This difference can be discussed in the following way: the critical overpotential for dendritic growth initiation in the systems where $j_L > j_0$ is given by Eq. (2.4):

$$\eta_i = \frac{b_c}{2.3} \ln \frac{j_L}{j_0} \quad (2.4)$$

and the critical overpotential for the instantaneous dendritic growth is given by Eq. (2.5):

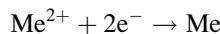
$$\eta_c = \frac{b_c}{2.3} \ln \left[\frac{j_L}{j_0} \left(\frac{\delta}{h} \right)^\gamma \right], \quad (2.5)$$

where δ is the diffusion layer thickness, and h is the height of protrusion from which the growth of dendrite commences and $\gamma = \frac{\text{dlog} j_0}{\text{dlog} c}$ [28].

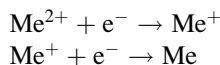
According to Newman [37];

$$j_0 \approx c^\gamma, \quad (2.6)$$

where $\gamma = 0.5$ [38] for



and $\gamma = 0.75$ [37] for



reaction mechanisms.

Taking into account Eqs. (2.1) and (2.6), one obtains

$$\frac{j_L}{j_0} \approx c^{n-\gamma}, \quad (2.7)$$

where $n - \gamma > 0$ in both cases.

From Eqs. (2.4), (2.5), and (2.7), it could be confirmed that in the activation–diffusion controlled electrodeposition, both η_i and η_c increase with increasing j_L/j_0 ratios (or with the decreasing j_0/j_L ratios). This means that increasing the concentration of the depositing ions leads to an increase in both η_i and η_c , as already observed in the case of copper electrodeposition [39].

On the other hand, if $j_L/j_0 \ll 1$ (very fast electrodeposition processes), Eqs. (2.4) and (2.5) become

$$\eta_i = \frac{RT}{nF} \frac{j_L}{j_0} \quad (2.8)$$

and

$$\eta_c = \frac{RT}{nF} \frac{j_L}{j_0} \left(\frac{\delta}{h} \right)^\gamma, \quad (2.9)$$

where nF is the number Faradays per mole of consumed ions, R is gas constant, and T is temperature. These relations show that dendritic growth is to be expected at very low overpotentials.

The difference between η_c and η_i can be written as

$$\eta_c - \eta_i = \frac{RT}{nF} \frac{j_L}{j_0} \left[\left(\frac{\delta}{h} \right)^\gamma - 1 \right] \quad (2.10)$$

from which it can be seen that this difference decreases with the decreasing j_L/j_0 value (or increasing j_0/j_L value). Hence, the difference between η_c and η_i decreases with increasing concentration of Pb(II) ions and becomes negligible at the sufficiently large concentrations of Pb(II) ions. In an ohmic-diffusion controlled electrodeposition process, the maximum current density corresponding to the ohmic controlled electrodeposition increases with increasing j_0/j_L ratio. This causes, after elimination of the ohmic potential drop, a decrease in both the overpotential at which electrodeposition system enters diffusion control, η_i and the overpotential at

which full diffusion control is attained, η_c , as well as of the difference between them, with the increasing concentration of Pb(II) ions.

In addition, a semiquantitative analysis of Eq. (2.10) confirms very well the presented results. As already mentioned, for fast electrochemical processes $j_0 \rightarrow \infty$ and $j_0 \gg j_L$ (or $j_L/j_0 \ll 1$). The j_L/j_0 ratio decreases with increasing concentration of Pb(II) ions and at the sufficiently high concentration of Pb(II) ions, this ratio will tend to zero ($j_L/j_0 \rightarrow 0$). Then, the right side of Eq. (2.10) will also tend to zero and hence $\eta_c - \eta_i \rightarrow 0$ (or $\eta_c \approx \eta_i$), which corresponds to full ohmic control of the electrodeposition process.

On the other hand, in the case of the electrodeposition under mixed activation–diffusion control ($j_0 < j_L$), the difference between η_c and η_i (Eqs. (2.4) and (2.5), respectively) could be presented by Eq. (2.11):

$$\eta_c - \eta_i = \frac{\gamma b_c}{2.3} \ln \frac{\delta}{h}. \quad (2.11)$$

It is very clear from Eq. (2.11) that this difference does not depend on the j_L/j_0 ratio and hence, on the concentration of the depositing ions. Furthermore, this difference will always have a finite value which will never tend to zero. This is one of the substantial differences between this electrodeposition system (activation–diffusion control of the electrodeposition; $j_0 < j_L$) and the one characterized by an extremely large exchange current density (ohmic–diffusion control of the electrodeposition; $j_0 \gg j_L$) from the point of view of the formation and growth of dendrites.

2.3 Correlation Between Polarization Characteristics and Morphology of Lead Deposits

2.3.1 Morphology of Lead Deposits Obtained from the Nitrate Electrolytes with the Different Concentration of Pb(II) Ions

One of the best ways to analyze an electrodeposition system is to establish a correlation between the polarization characteristics and the morphology of the deposits. All electrodepositions which results are presented in this chapter were performed in an open cell at room temperature from the corresponding solutions [32]. Lead was electrodeposited on vertical cylindrical copper electrodes, while the reference and counter electrodes were of pure lead.

The solution containing 0.30 M Pb(NO₃)₂ in 2.0 M NaNO₃ was taken as the basic solution for the determination of this correlation.

Figure 2.9 shows the morphologies of lead deposits electrodeposited from 0.30 M Pb(NO₃)₂ in 2.0 M NaNO₃ at overpotentials corresponding to ohmic

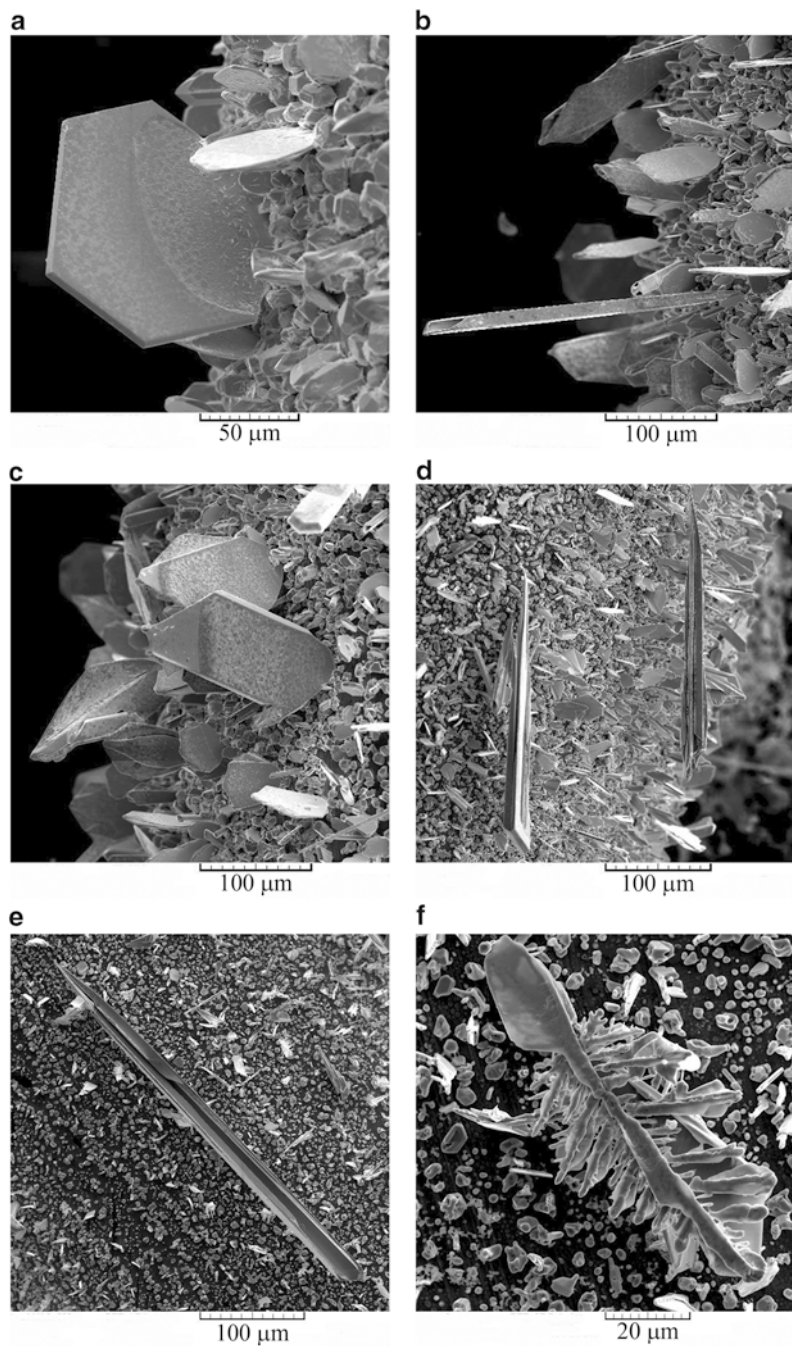


Fig. 2.9 Morphologies of lead deposits obtained from 0.30 M $\text{Pb}(\text{NO}_3)_2$ in 2.0 M NaNO_3 at overpotentials, η of: (a) 30 mV, (b) and (c) 55 mV, (d) 80 mV, (e) and (f) 120 mV (Reprinted from [32] with permission from Elsevier.)

controlled electrodeposition ($\eta = 30$ mV; Fig. 2.9a), the end of the limiting diffusion current density plateau ($\eta = 55$ mV; Fig. 2.9b, c), and during the fast increase in the current density with increasing overpotential ($\eta = 80$ mV; Fig. 2.9d, and $\eta = 120$ mV; Fig. 2.9e, f).

Individual regular crystals were formed at an overpotential of 30 mV, i.e., when the electrodeposition was ohmic control (Fig. 2.9a). Apart from individual regular lead crystals, crystals of irregular shape and needle-like dendrites were formed during electrodeposition at an overpotential corresponding to the end of the limiting diffusion current density plateau (Fig. 2.9b, c). Needle-like dendrites were dominantly formed at an overpotential of 80 mV (Fig. 2.9d), which was 25 mV greater than the overpotential corresponding to the inflection point. These types of dendrites were also formed at an overpotential of 120 mV (Fig. 2.9e) but, in addition, fern-like dendrites were formed as well (Fig. 2.9f).

In order to gain a comprehensive insight into the effect of the concentration of Pb (II) ions on the morphology of the lead deposits, the obtained surface morphologies were compared with those obtained from 0.050 to 0.45 M $\text{Pb}(\text{NO}_3)_2$ in 2.0 M NaNO_3 at some of the above-employed overpotentials.

The morphologies of the lead deposits electrodeposited from 0.050 M $\text{Pb}(\text{NO}_3)_2$ in 2.0 M NaNO_3 at overpotentials of 30, 55, and 80 mV are shown in Figs. 2.10 and 2.11. Crystals of irregular shape and dendritic forms were formed at $\eta = 30$ mV (Fig. 2.10a–c). The lead crystals formed from this solution were narrower and more elongated than those formed by electrodeposition from 0.30 M $\text{Pb}(\text{NO}_3)_2$ in 2.0 M NaNO_3 , and could be considered as precursors of dendrites [30, 31]. During lead electrodeposition from 0.050 M $\text{Pb}(\text{NO}_3)_2$ in 2.0 M NaNO_3 , the formation of dendritic forms and precursors of dendrites at $\eta = 30$ mV is understandable because this overpotential belongs to the plateau of the limiting diffusion current density (Figs. 2.1a and 2.2a). Aside from irregular crystals, needle-like and fern-like dendrites were formed at the overpotential corresponding to the end of the limiting diffusion current density plateau ($\eta = 55$ mV; Fig. 2.10d, e). It is necessary to note that the fern-like dendrite shown in Fig. 2.10e developed from an individual lead crystal. A similar development of a fern-like dendrite was also observed during electrodeposition from 0.30 M $\text{Pb}(\text{NO}_3)_2$ in 2.0 M NaNO_3 at $\eta = 120$ mV (Fig. 2.9f).

The morphology of the electrodeposited lead obtained from 0.050 M $\text{Pb}(\text{NO}_3)_2$ in 2.0 M NaNO_3 at an overpotential of 80 mV is shown in Fig. 2.11. The dendrites formed under these electrodeposition conditions were completely different from those already observed and analyzed. These dendrites consisted of a beam of saw-like forms. A similar surface morphology was also obtained by lead electrodeposition from this solution at overpotentials larger than 80 mV.

Lead deposits obtained from 0.45 M $\text{Pb}(\text{NO}_3)_2$ in 2.0 M NaNO_3 at overpotentials of 55, 80, and 120 mV are shown in Fig. 2.12. Individual regular crystals were formed at an overpotential of 55 mV, corresponding to the end of ohmic control of electrodeposition (Fig. 2.12a). The numerous elongated crystals (precursors of dendrites) were formed by electrodeposition at 80 mV (Fig. 2.12b). Finally, a

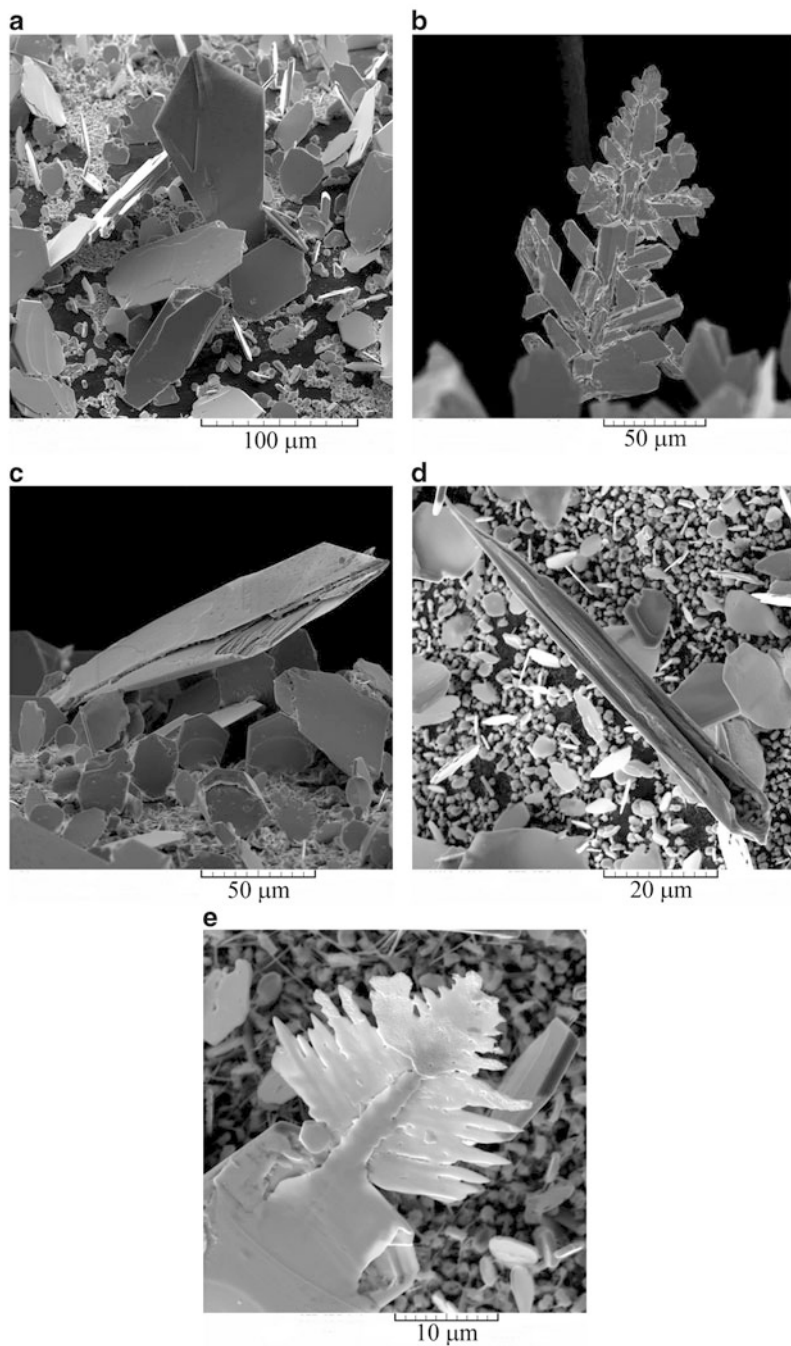


Fig. 2.10 Morphologies of lead deposits obtained from 0.050 M $\text{Pb}(\text{NO}_3)_2$ in 2.0 M NaNO_3 at overpotentials, η of: (a), (b), and (c) 30 mV, (d) and (e) 55 mV (Reprinted from [32] with permission from Elsevier.)

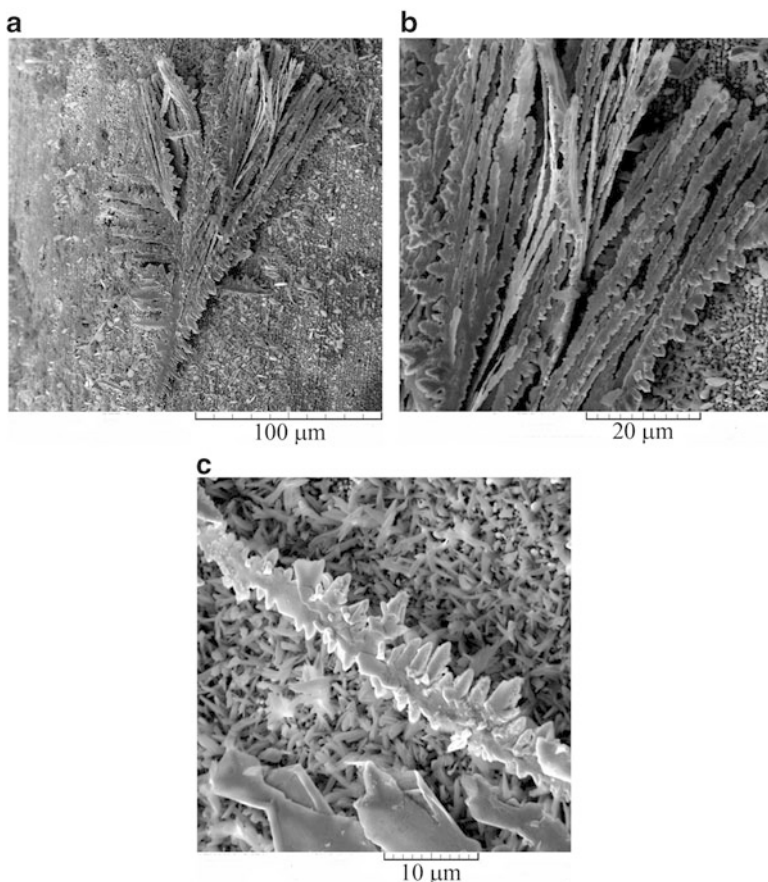


Fig. 2.11 Morphologies of lead deposits obtained from 0.050 M $\text{Pb}(\text{NO}_3)_2$ in 2.0 M NaNO_3 at an overpotential, η , of 80 mV (Reprinted from [32] with permission from Elsevier.)

mixture of needle-like and fern-like dendrites was formed by lead electrodeposition at an overpotential of 120 mV (Fig. 2.12c, d, respectively).

An analysis of the polarization characteristics and morphologies of lead deposits showed that in the mixed ohmic-diffusion control of the electrodeposition process, dendritic growth is initiated at overpotentials belonging to the diffusion part of the polarization curve. Therefore, as in the case of the diffusion controlled electrodeposition, the overpotential at which the system enters diffusion control can be denoted as the critical overpotential for dendritic growth initiation, η_i , while the overpotential at which diffusion control becomes complete can be denoted as the critical overpotential for instantaneous dendritic growth, η_c . Morphological analysis of electrodeposited lead showed that the critical overpotential for instantaneous dendritic growth, η_c , corresponds to the inflection point on the polarization curve. The difference between η_i and η_c decreases with increasing concentration of Pb

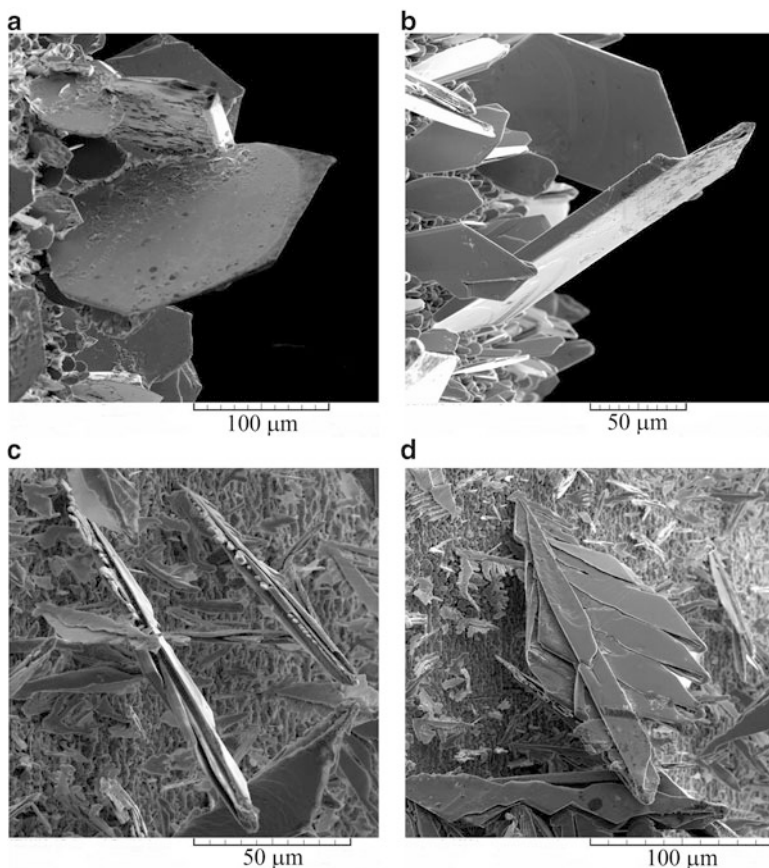


Fig. 2.12 Morphologies of lead deposits obtained from 0.45 M $\text{Pb}(\text{NO}_3)_2$ in 2.0 M NaNO_3 at overpotentials, η , of: (a) 55 mV, (b) 80 mV, and (c) and (d) 120 mV (Reprinted from [32] with permission from Elsevier.)

(II) ions and finally they become the same when complete ohmic control of the electrodeposition process is attained. In this way, it is experimentally proven that the inflection point on the polarization curve for the case of full ohmic control of the electrodeposition process corresponds to the condition $\eta_i = \eta_c$.

Increasing the concentration of $\text{Pb}(\text{II})$ ions led to a shift of the formation of characteristic morphological forms towards higher electrodeposition overpotentials. As already observed, fern-like dendrites were formed from 0.050 M $\text{Pb}(\text{NO}_3)_2$ in 2.0 M NaNO_3 at $\eta = 55$ mV, while this shape of dendrites was formed from 0.30 M $\text{Pb}(\text{NO}_3)_2$ in 2.0 M NaNO_3 at $\eta = 120$ mV. On the other hand, regular crystals were formed from 0.45 M $\text{Pb}(\text{NO}_3)_2$ in 2.0 M NaNO_3 at $\eta = 55$ mV, while this morphological form was obtained at $\eta = 30$ mV from 0.30 M $\text{Pb}(\text{NO}_3)_2$ in 2.0 M NaNO_3 . The same trend in the development of surface morphology was also observed during copper electrodeposition from solutions of different CuSO_4 concentrations [39].

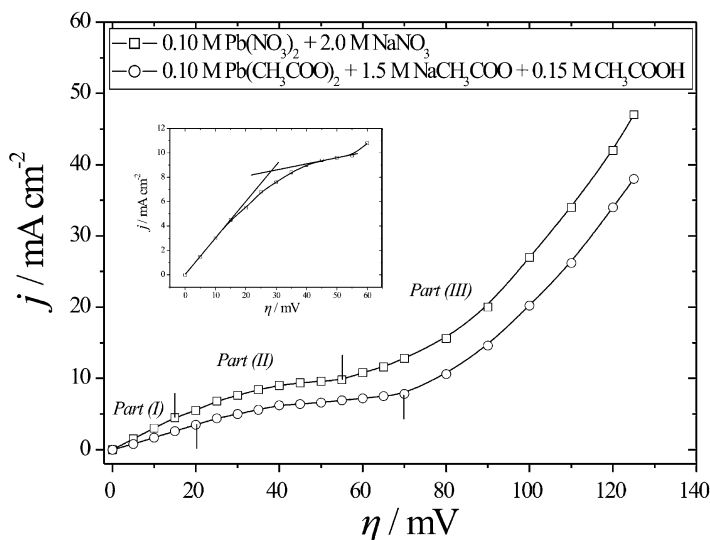


Fig. 2.13 The polarization curves for lead electrodeposition from 0.10 M $\text{Pb}(\text{CH}_3\text{COO})_2 + 1.5 \text{ M NaCH}_3\text{COO} + 0.15 \text{ M CH}_3\text{COOH}$ and 0.10 M $\text{Pb}(\text{NO}_3)_2 + 2.0 \text{ M NaNO}_3$ (Reprinted from [43] with permission from Elsevier.)

2.3.2 Comparison of Lead Electrodeposition Processes from the Basic (Nitrate) and Complex (Acetate) Electrolytes

The complex electrolytes represent the special type of electrolytes, and they can be from the group of both acid and alkaline ones. In the metal electrodeposition processes, the effect of complex formation is limited not only on the polarization behavior of the metal [31, 40], but to the morphology of metal deposits, as observed in the production of silver [31, 40, 41] and bismuth [42] powdered deposits.

2.3.2.1 Comparative Analysis of the Polarization Curves

The polarization curves for lead electrodeposition from the basic (nitrate) and complex (acetate) electrolytes are shown in Fig. 2.13. The polarization curves were recorded on cylindrical copper electrodes using experimental procedure described in Sect. 2.2.1. Similar to the polarization curve recorded from the nitrate electrolyte, the polarization curve recorded from the acetate electrolyte also consisted of three parts. These three parts are clearly denoted in Fig. 2.13.

The characteristic of the first part (*Part (I)*) is the linear dependence of the current density on overpotential and, as already mentioned, this linear part corresponds to the ohmic controlled electrodeposition process. With the nitrate ions used, the interval of overpotentials corresponding to the ohmic control is between

0 and 15 mV. When the acetate ion was used, the end of the ohmic control of the electrodeposition corresponded to an overpotential of 20 mV.

The second part of the polarization curves (*Part (II)*) corresponds to the diffusion controlled electrodeposition process. The ranges of overpotentials belonging to the diffusion control of the electrodeposition are from 15 to 55 mV for the basic electrolyte and from 20 to 70 mV for the complex electrolyte. The beginning of the plateau of the limiting diffusion current density is determined as intersect of straight lines joining current densities in the ohmic and diffusion control of electrodeposition, as inserted in Fig. 2.13. The plateaus of the limiting diffusion current density, determined in this way, were between 28.5 and 55 mV for the nitrate electrolyte and between 33 and 70 mV for the acetate electrolyte.

The inflection point at the polarization curves denoted the ends of the plateau of the limiting diffusion current density. The fast increase of the current density after the inflection point is the characteristic of the third part of the polarization curves (*Part (III)*). The inflection point corresponds to an overpotential of 55 mV for the nitrate and 70 mV for the acetate electrolytes.

The electrical conductivities of the electrolytes were 4.22 mS for the nitrate electrolyte and 7.06 mS for the acetate electrolyte. As seen from Fig. 2.13, this noticeable increase of the electrical conductivity of the acetate electrolyte of about 40 % showed the strong effect on the polarization characteristics of lead electrodeposition system.

The following differences in the polarization curves obtained from the basic (nitrate) and complex (acetate) electrolytes were observed [43]: (a) the intervals of overpotentials corresponding to the both ohmic and diffusion controls of the electrodeposition were larger for the complex than for the basic electrolytes, and (b) the plateau of the limiting diffusion current density was wider for the complex than for the basic electrolytes. The smaller value of the limiting diffusion current density for the complex electrolyte (for about 27 %) is probably due to the decrease of diffusion coefficient caused by the process of complexing of Pb (II) ions.

2.3.2.2 Comparative Analysis of Morphologies of Lead Deposits

In the next step, the polarization characteristics were correlated with morphologies of lead deposits obtained by the electrodeposition processes at overpotentials corresponding to the different positions at the polarization curves. In this way, the very important information related with the type of used electrolytes was obtained.

Figure 2.14 shows morphologies of lead deposits obtained at an overpotential of 10 mV belonging to the ohmic controlled electrodeposition for the basic (Fig. 2.14a) and complex (Fig. 2.14b) electrolytes. In both cases, the individual regular crystals were formed. It is necessary to note that the formed regular crystals were very similar to each others.

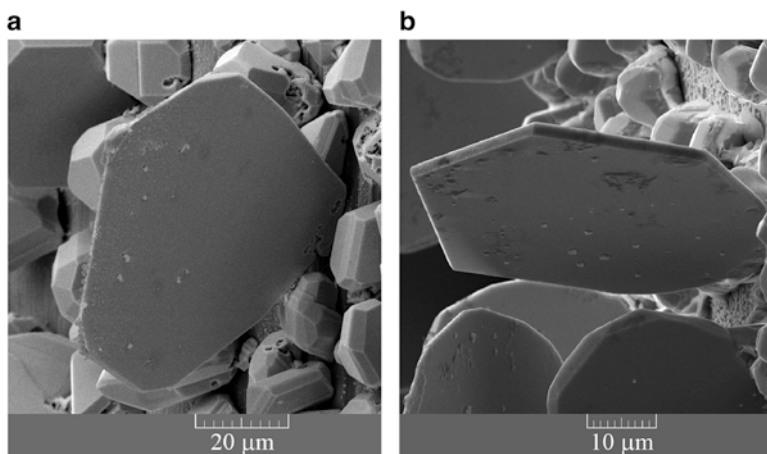


Fig. 2.14 Morphologies of electrodeposited lead obtained in the ohmic controlled electrodeposition at $\eta = 10$ mV from: (a) 0.10 M $\text{Pb}(\text{NO}_3)_2 + 2.0$ M NaNO_3 and (b) 0.10 M $\text{Pb}(\text{CH}_3\text{COO})_2 + 1.5$ M $\text{NaCH}_3\text{COO} + 0.15$ M CH_3COOH (Reprinted from [43] with permission from Elsevier.)

Morphologies of electrodeposited lead obtained at the plateaus of the limiting diffusion current density ($\eta = 50$ mV) from the both solutions are shown in Fig. 2.15. The regular crystals, different irregular forms denoted as precursors of dendrites (Fig. 2.15a), and the needle-like dendrites (Fig. 2.15b) were formed by the electrodeposition from the nitrate electrolyte. The regular crystals and needle-like dendrites were also formed by the electrodeposition from the acetate solution (Fig. 2.15c). However, aside from these morphological forms, the use of the acetate electrolyte led to the formation of the fern-like dendrites during the electrodeposition process at $\eta = 50$ mV (Fig. 2.15d).

The number of the formed fern-like dendrites increased with the increase of overpotential of electrodeposition inside the plateau of the limiting diffusion current density (Fig. 2.16a–c). From Fig. 2.16 which shows the fern-like dendrites electrodeposited at an overpotential of 60 mV from the acetate electrolyte can be clearly seen that these fern-like dendrites were more branchy structures than those formed at 50 mV. The regular crystals, the precursors of dendrites, and the needle-like dendrites can be also obtained by the electrodeposition at this overpotential (Fig. 2.16d).

The typical surface morphologies of lead obtained by the electrodeposition processes at an overpotential of 100 mV which belong to the third part of the polarization curves are shown in Figs. 2.17 (the nitrate electrolyte) and 2.18 (the acetate electrolyte). Although dendrites are formed by the electrodeposition processes from the both solutions, the difference between them was very evident.

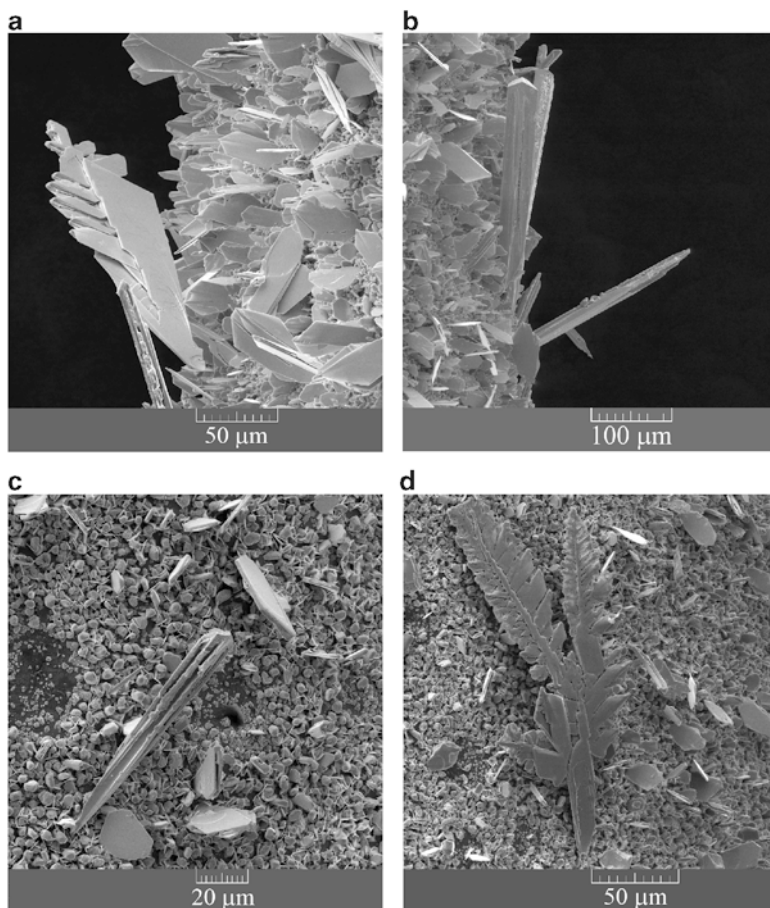


Fig. 2.15 Morphologies of electrodeposited lead obtained at the plateaus of the limiting diffusion current density ($\eta = 50$ mV) from: (a) and (b) $0.10 \text{ M Pb(NO}_3)_2 + 2.0 \text{ M NaNO}_3$, (c) and (d) $0.10 \text{ M Pb(CH}_3\text{COO)}_2 + 1.5 \text{ M NaCH}_3\text{COO} + 0.15 \text{ M CH}_3\text{COOH}$ (Reprinted from [43] with permission from Elsevier.)

The mixture of needle-like and the fern-like dendrites was obtained at an overpotential of 100 mV when the nitrate solution was used (Fig. 2.17). However, these fern-like dendrites were completely different of those obtained from the acetate electrolyte at $\eta = 60$ mV (Fig. 2.16), as well as of those formed from the same electrolyte at $\eta = 100$ mV (Fig. 2.18). As shown in Fig. 2.18, the very branchy fern-like dendrites, similar to those obtained at $\eta = 60$ mV, were obtained by the electrodeposition from the acetate solution at an overpotential of 100 mV.

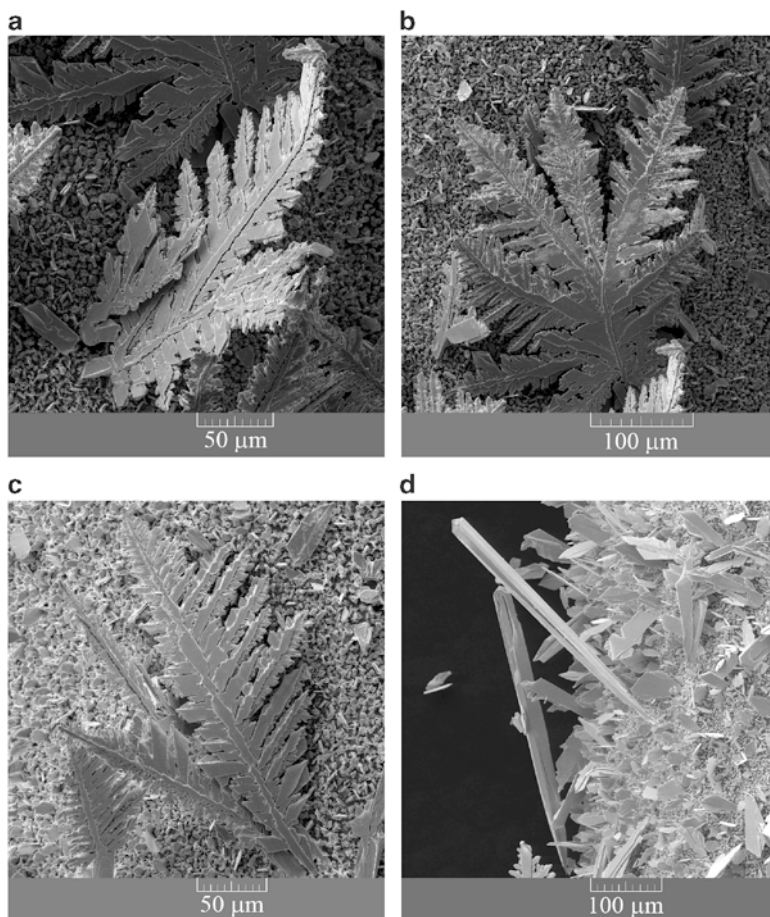


Fig. 2.16 (a)–(c) The fern-like dendrites and (d) the precursors of dendrites and the needle-like dendrites electrodeposited at an overpotential of 60 mV from 0.10 M $\text{Pb}(\text{CH}_3\text{COO})_2$ + 1.5 M NaCH_3COO + 0.15 M CH_3COOH (Reprinted from [43] with permission from Elsevier.)

2.3.3 *General Discussion of the Correlation Between the Polarization Characteristics and Morphologies of Lead Deposits Obtained from the Different Electrolytes*

For the purpose of easier analysis of lead electrodeposition processes from the basic and complex electrolytes, the comparative survey of the polarization characteristics and the typical morphologies of lead deposits is shown in Fig. 2.19.

Electrodeposition of lead from the both electrolytes occurs in the conditions of the mixed ohmic-diffusion control of the electrodeposition process. The shape of

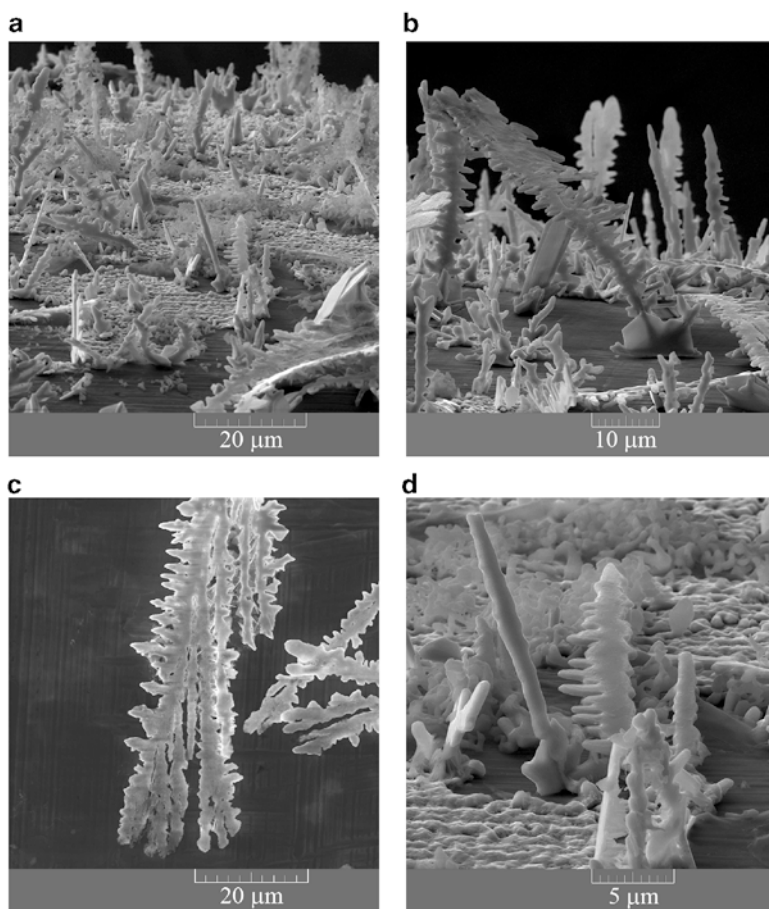


Fig. 2.17 Lead dendrites formed at an overpotential of 100 mV from 0.10 M $\text{Pb}(\text{NO}_3)_2$ + 2.0 M NaNO_3 (Reprinted from [43] with permission from Elsevier.)

regular crystals formed in the ohmic control of the electrodeposition (Fig. 2.14) did not depend on the type of used electrolytes. On the other hand, the shape of dendrites was strongly affected by the type of electrolytes. Lead dendrites obtained from the nitrate solution were less branchy and completely different form than those obtained from the acetate solution. The common characteristic of all lead morphological forms is their 2D (two-dimensional) form. The shape of the dendrites formed from the nitrate solution was similar to silver dendrites [31, 40], while the dendrites formed from the acetate solution were very similar to cadmium dendrites [44]. The needle-like dendrites like those obtained from the both nitrate and acetate solutions were also observed during tin electrodeposition [45]. This similarity in the shape of dendrites is understandable because all the above-mentioned metals belong to the same group of metals (“normal metals”) in Winand’s classification of metals [7].

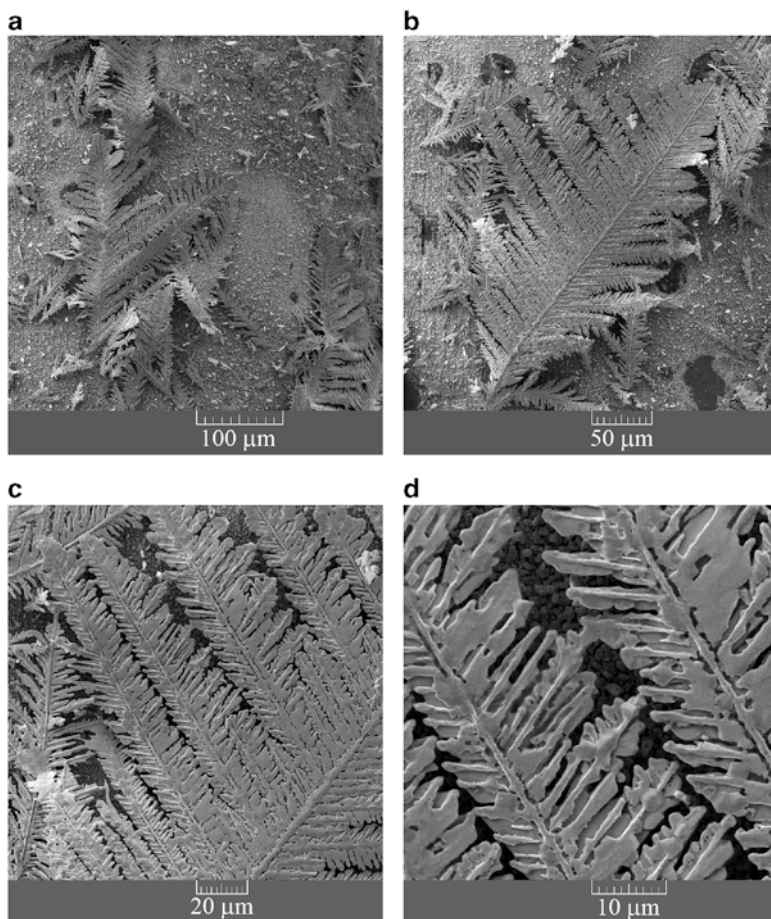


Fig. 2.18 Lead dendrites formed at an overpotential of 100 mV from 0.10 M $\text{Pb}(\text{CH}_3\text{COO})_2$ + 1.5 M NaCH_3COO + 0.15 M CH_3COOH (Reprinted from [43] with permission from Elsevier.)

It is very clear that the classical Wranglen's definition of a dendrite can be applied to all the above observed dendritic forms. According to Wranglen [46], a dendrite consists of a stalk and of branches (primary, secondary, etc.) and resembles a tree. The flat and fern-like dendrites are referred as two-dimensional (2D) dendrites. The dendrite consisting only of the stalk and primary branches are referred as primary (P) dendrite. If the primary branches in turn develop secondary branches, the dendrite is called secondary (S). It is very clear from the above consideration that the needle-like dendrites are composed only of stalk (Figs. 2.9d, e, 2.10d, 2.12c, 2.15b, c, 2.16d, and 2.17a, d). From Figs. 2.9f, 2.10e, 2.12d, and 2.17b, c, it can be seen that the primary type of dendrites was formed by the electrodeposition from the basic nitrate solution. The primary branches are poorly developed, and this type of primary branches can be denoted as

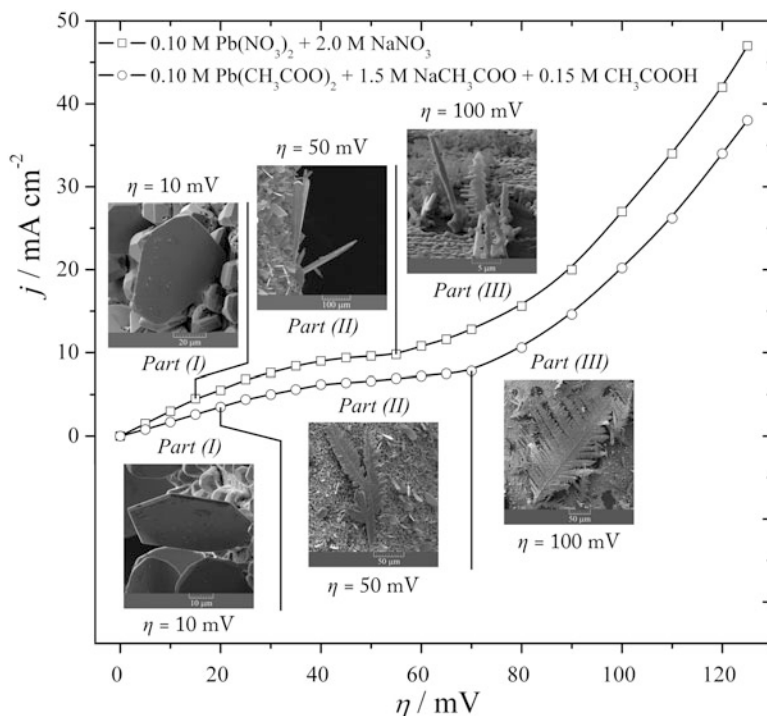


Fig. 2.19 The comparative survey of the polarization curves and the typical morphologies of lead deposits electrodeposited from 0.10 M $\text{Pb}(\text{NO}_3)_2 + 2.0 \text{ M NaNO}_3$ and 0.10 M $\text{Pb}(\text{CH}_3\text{COO})_2 + 1.5 \text{ M NaCH}_3\text{COO} + 0.15 \text{ M CH}_3\text{COOH}$ (Reprinted from [43] with permission from Elsevier.)

“tooth of saw” [32, 43]. On the other hand, the secondary type of dendrites was formed by the electrodeposition from the complex acetate solution (Fig. 2.18). In this type of dendrite, the primary branches were very well developed, and the secondary type of branches was developed from these primary branches.

From the electrochemical point of view, a dendrite is defined as an electrode surface protrusion that grows under activation control, while electrodeposition to the macroelectrode is predominantly under diffusion control [27, 28, 44, 47–49]. Dendritic growth is initiated at some overpotential belonging to the diffusion part at the polarization curve. The simultaneous formation of the various irregular forms from regular crystals and precursors of dendrites to the both needle-like and fern-like dendrites clearly confirms the fact that the critical overpotential for dendritic growth initiation, η_i , belongs to the diffusion part of the polarization curve, and that it denotes overpotential at which the system enters diffusion control of the electrodeposition. The outer limit of the diffusion layer of the macroelectrode was not disrupted during formation of these irregular morphological forms. The critical overpotential for instantaneous dendritic growth, η_c , is overpotential at which diffusion control becomes complete, and this overpotential

corresponds to the inflection point at the polarization curve [32]. The formation of only dendritic forms at an overpotential of 100 mV just confirmed this assumption.

Finally, after the inflection point, the electrodeposition systems remain diffusion controlled ones, and the rapid increase of the current density after the inflection point is a result of the fast growth of dendrites and strong increase of the surface area. Then, using the electrochemical definition of a dendrite, it follows that this sudden and rapid increase of the current density with the increasing overpotential after the inflection point [*Part (III)* in the polarization curves] can be mainly ascribed to the activation controlled electrodeposition at the tips of the formed dendrites. It is very clear that the tips of both primary and secondary branches contribute to the overall control of electrodeposition process causing the disruption of the outer limit of the diffusion layer of the macroelectrode.

In summary, the following differences in the polarization and morphological characteristics between the complex (acetate) and basic (nitrate) electrolytes were observed:

- (a) The increase of the plateau of the limiting diffusion current density and the shift of the inflection point to the higher overpotential of electrodeposition
- (b) Formation of more branchy dendrites from the complex electrolyte (the secondary (S) type) in relation to those formed from the basic (nitrate) electrolyte (the primary (P) type).

These differences can be ascribed to the lower exchange current density, j_0 , and hence, to the lower rate of the electrochemical process for the complex acetate electrolyte than for the basic nitrate electrolyte. The proof that the processes of complex formation lowers the exchange current density can be found in the comparison with silver electrodeposition processes from the nitrate and ammonium electrolytes [31, 40]. Electrodeposition of silver from the nitrate electrolytes, similar to lead electrodeposition, belongs to the fast electrochemical processes characterized by $j_0 \rightarrow \infty$ [7, 27, 28, 30, 47]. On the other hand, ammonium ions makes complex with Ag(I) ions approaching the polarization and morphological characteristics of silver to those of copper [50–56]. In this way, it is enabled the determination of j_0 from the intercept of anodic and cathodic Tafel slopes [57]. For metals like copper and silver (the ammonium complex), the determined exchange current density values, j_0 , were smaller than the limiting diffusion current density, j_L ($j_0 < j_L$), and these metals, together with Au, are classified in the group of intermediate metals (Winand's classification of metals) [7]. This considerably decrease of the exchange current density by the complexing process was manifested by the increase of the plateau of the limiting diffusion current density (from 75–175 mV for the basic nitrate electrolyte to 250–700 mV for the ammonium complex electrolyte [31, 40, 58]), and by the strong ramification of silver dendrites and by the change of their shape of those like lead electrodeposited from the nitrate electrolyte (Fig. 2.17) to those similar to copper [50–56, 59, 60].

This analysis enables to make an analogy with lead electrodeposition processes from the basic and complex electrolytes. It is necessary because there is no a precise and reference method for the determination of the exchange current density for the

majority of normal metals, such as Pb, Ag, Sn, and Zn, characterized by the extremely large exchange current density. For these metals, the exchange current density values are referred as $j_0 \rightarrow \infty$. For that reason, it is necessary to find some auxiliary criteria for the comparison of electrodeposition systems characteristic by $j_0 \rightarrow \infty$ with point of view of the different j_0 values (i.e., rate of electrochemical process). It is very clear from the above consideration that the method based on the comparison of polarization and morphological characteristics of the different systems can be a very suitable way for this analysis. In this way, it can be concluded that the increase of the plateau of the limiting diffusion current density and the formation of more branchy lead dendrites from the acetate electrolyte than those formed from the nitrate one can be definitely ascribed to the lower exchange current density for the acetate complex electrolyte than for the basic nitrate electrolyte.

The another proof that the lead electrochemical system based on the acetate ions has lower exchange current density than the one based on the nitrate ions can be derived on the basis of similarity with the shape of silver and cadmium dendrites. The silver dendrites electrodeposited from the nitrate solution [31, 40] were similar to lead dendrites obtained from the nitrate solution (Figs. 2.9f, 2.10e, 2.12d, and 2.17). The exchange current density for silver (from the silver nitrate solution) was estimated to be between 1 and 7 A/cm² [38]. On the other hand, the cadmium dendrites [44] were very similar to the lead dendrites obtained from the acetate solution (Fig. 2.18). The exchange current density for the cadmium system was estimated to be 1.5×10^{-3} A/cm² [47, 61], which was for about one thousand and more smaller than the one for silver.

Also, it can be supposed that the degree of the change of the both polarization and morphological characteristics is closely related with the stability of formed complexes. Namely, Pb(II) ions form relatively weak complexes with acetate ions, and the relatively small increase of the plateau of the limiting diffusion current density was observed in the relation to the basic electrolyte. The stability constant for these complexes are $\log K_1 = 2.33$ and $\log \beta_2 = 3.60$. Contrary, the ammonium ions make the strong complex with Ag(I) ions, which is followed by the considerable increase of the plateau of the limiting diffusion current density. The stability constant for these complexes are $\log K_1 = 3.24$ and $\log \beta_2 = 7.24$. Hence, the stronger complex is formed, the stronger effect on the polarization characteristics and surface morphology of powder particles is observed.

The final morphology of electrodeposited lead was determined by overpotential and the composition of solution. However, the complete insight in the mechanism of lead electrodeposition processes and formation of different morphological forms from regular crystals to dendrites cannot be obtained without knowledge of the phenomena related with the process of nucleation. Mostany et al. [13] investigated the nucleation of lead onto vitreous carbon electrodes from the solutions of the different Pb(NO₃)₂ concentrations in 1.0 M KNO₃ and they found that the number density of active sites for nucleation increases with overpotential. Also, the number density of active sites is approximately constant at a given overpotential and it is independent of concentration of Pb(II) ions. The type of nucleation changed from

progressive nucleation in the most dilute solution to instantaneous nucleation in more concentrated one. Considering the fact that the number of active sites was found to be independent of concentration, the transition from a progressive nucleation regime in dilute solutions to instantaneous at higher concentrations indicates that the nucleation rates increased with concentration [13]. The type of nucleation is related with the initial stages of electrodeposition (less than 0.5 s), while the final surface morphology is not only determined by overpotential and the composition of solution but also to the time of electrodeposition and the type of working electrode. Anyway, the number of formed regular crystals, dendrites, and the other irregular forms depend on the number density of active sites indicating on a close correlation between the nucleation process and the final morphology of electrodeposited lead.

2.4 Correlation Between the Morphology of Lead Deposits and the Crystallographic Structure

Electrodeposition of lead from 0.45 M $\text{Pb}(\text{NO}_3)_2$ in 2.0 M NaNO_3 is the typical representative of the ohmic controlled electrodeposition with the inflection point at an overpotential of 55 mV (Fig. 2.1b).

The regular individual crystals of lead formed in the ohmic control at an overpotential of 20 mV are shown in Fig. 2.20 [62].

Electrodeposition process at an overpotential of 80 mV led to the formation largely irregular individual crystals (precursors of dendrites) as shown in Fig. 2.21. The increase of overpotential of electrodeposition from 80 to 140 mV led to the formation of different dendritic forms (Fig. 2.22). The two types of dendrites were formed by the electrodeposition at 140 mV: needle-like and fern-like dendrites.

Anyway, the two limiting morphological forms were obtained by the processes of lead electrodeposition from the concentrated nitrate solution—the individual

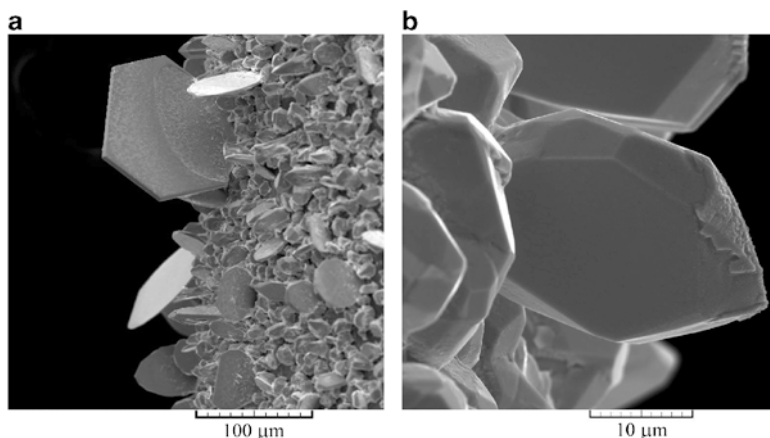


Fig. 2.20 Morphologies of lead deposits obtained from 0.45 M $\text{Pb}(\text{NO}_3)_2$ in 2.0 M NaNO_3 at an overpotential, η , of 20 mV

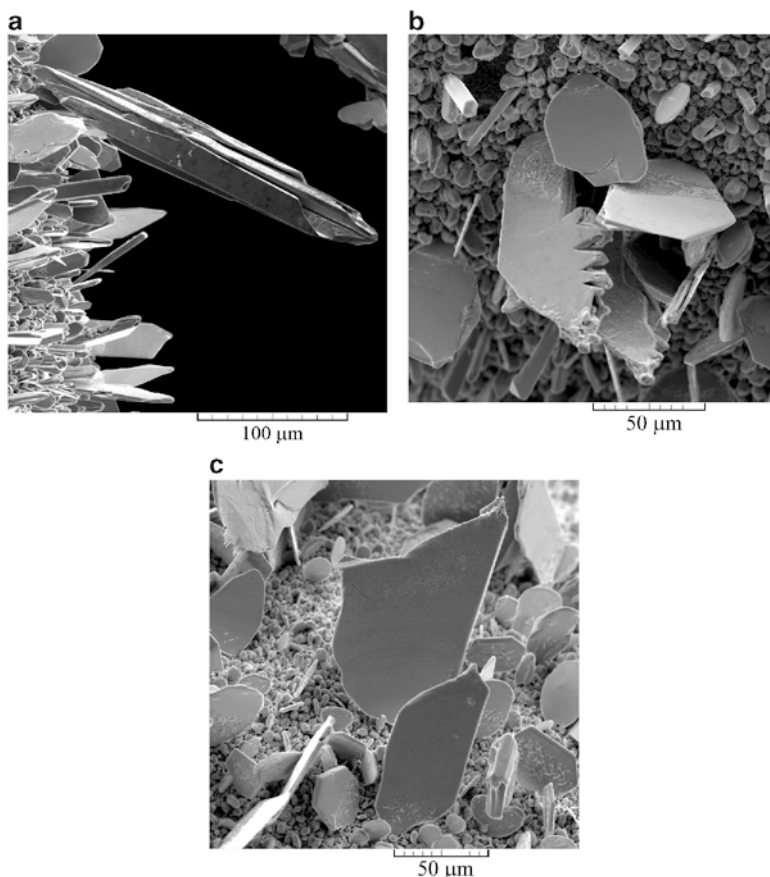


Fig. 2.21 Morphologies of lead deposits obtained from 0.45 M $\text{Pb}(\text{NO}_3)_2$ in 2.0 M NaNO_3 at an overpotential, η , of 80 mV (Reproduced from [62] by permission of The Royal Society of Chemistry.)

crystals in the ohmic controlled electrodeposition (Fig. 2.20) and the dendrites in the activation controlled electrodeposition at their tips (Fig. 2.22).

Powder particles for the X-ray diffraction (XRD) analysis were obtained by tapping the lead deposits shown in Figs. 2.20, 2.21, and 2.22, and the corresponding XRD patterns are shown in Fig. 2.23. The crystallites of Pb obtained at an overpotential of 20 mV were predominately oriented in the (111) plane. The ratio of crystallites oriented in the other planes was negligible. Aside from the dominant orientation of Pb crystallites in the (111) plane, the presence of Pb crystallites oriented in the (200), (220), (311), and (331) planes was observed in the XRD patterns of powder particles obtained at overpotentials of 80 and 140 mV. The ratio of crystallites oriented in these planes increased with the increase of overpotential of electrodeposition from 80 to 140 mV. Anyway, the strong preferred orientation in the (111) plane was observed in all electrodeposited forms.

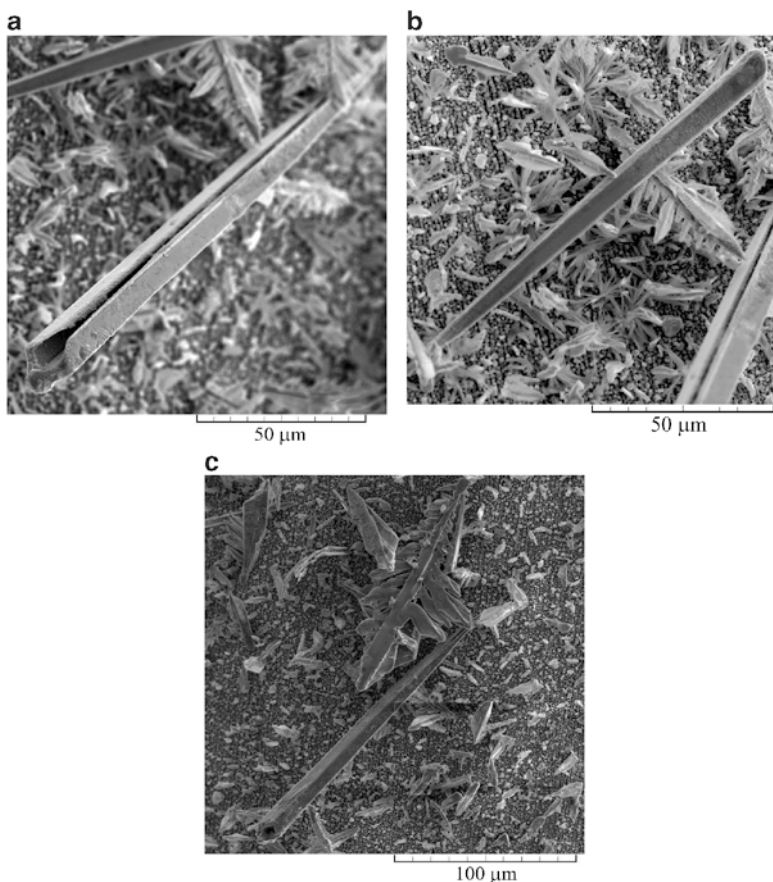


Fig. 2.22 Morphologies of lead deposits obtained from 0.45 M $\text{Pb}(\text{NO}_3)_2$ in 2.0 M NaNO_3 at an overpotential, η , of 140 mV

Analysis of Figs. 2.20, 2.21, 2.22, and 2.23 enables to correlate morphologies of lead deposits with its crystallographic structure. Then, formation of the different morphological forms from the regular crystals to dendrites of the different shape with the strong (111) preferred orientation can be discussed by the following consideration of general characteristics of growth layers in electrodeposition processes: lead crystallizes in a face-centered cubic (FCC-type) lattice, and Fig. 2.24 shows a crystal with a simple cubic lattice and (100), (111), and (110) faces [63]. The planes of the growth layers are the closely packed atom plane of the crystal lattice [46]. The growth layers start from certain active centers or growth centers on the crystal face. The beginning of growth layers is mainly determined by a current density or overpotential. At low current densities and overpotentials, the growth layers are invariably originated in the interior of the crystal faces, and a new layer is not started until the former has reached the edges of the crystal. At higher

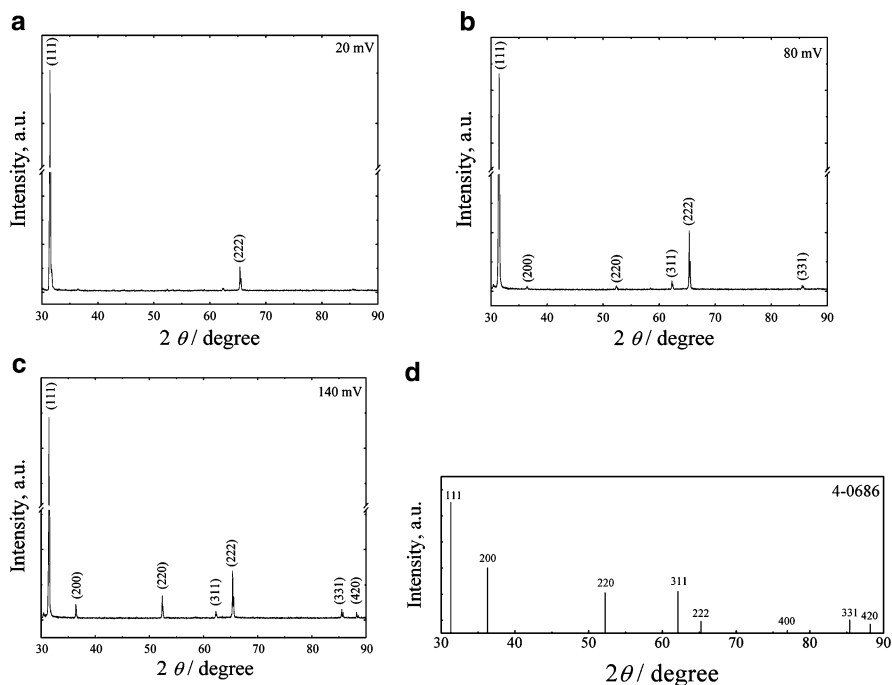
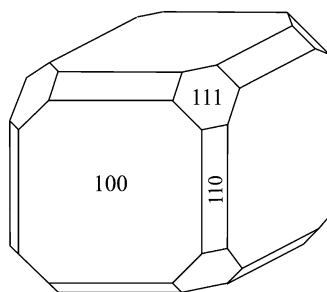


Fig. 2.23 The XRD patterns of the powder particles obtained by tapping the lead deposits electrodeposited at overpotentials of: (a) 20 mV, (b) 80 mV, and (c) 140 mV, and (d) for standard for Pb powder

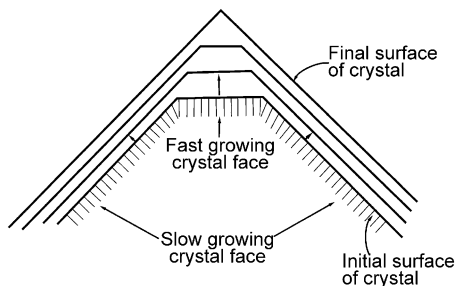
Fig. 2.24 A crystal with a simple cubic lattice and (100), (111), and (110) faces (According to [63]) (Reproduced from [62] by permission of The Royal Society of Chemistry.)



current densities and overpotentials when dendrites begin to form, growth centers are also observed at the edges and corners. In this case, new layers are developed before the forerunners have reached their final size so that at certain times a great many layers may be flowing simultaneously.

Hence, the origin of the growth layers is of both growth centers present in the interior of the crystal faces (center type; these growth layers are formed at low current densities and overpotentials) and growth centers present on the edges and

Fig. 2.25 The growth of a crystal illustrating how a fast-growing face grow out of existence, while the slow-growing crystal faces remain (According to [64]) (Reprinted from [65] with permission from Serbian Chemical Society.)



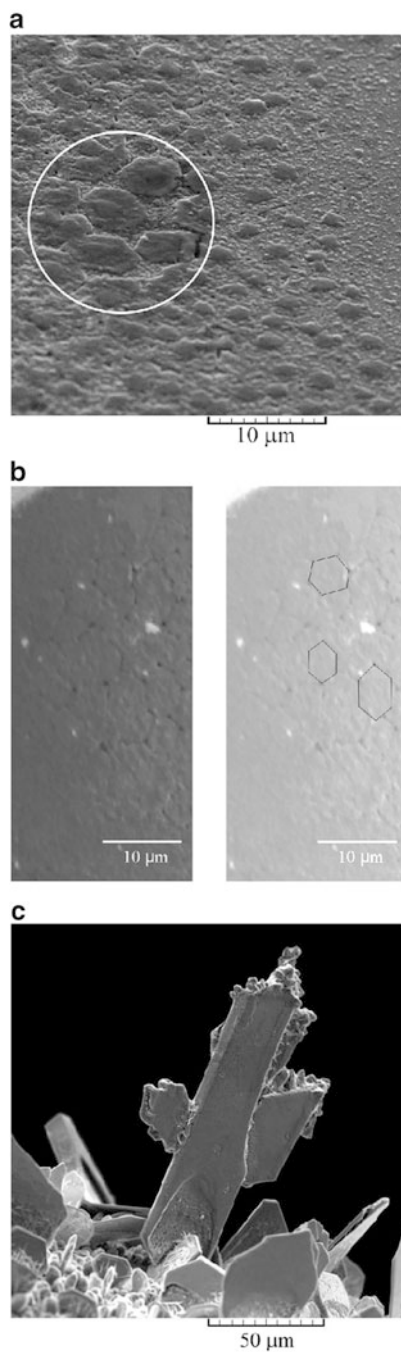
corners (edge and corner type; these growth layers are formed at high current densities and overpotentials).

At constant overpotential, the rates of electrodeposition for a FCC lattice increase in the order of $(110) > (100) > (111)$ [64]. This different deposition rate onto different faces had an important consequence; fast-growing faces tend to grow out of existence and disappear, and slow-growing faces tend to survive [64], as illustrated in Fig. 2.25.

The individual regular crystals shown in Fig. 2.20 are formed at the low overpotential ($\eta = 20$ mV), and hence, the growth centers present in the interior of the crystal faces (center type) are only responsible for their formation. During the electrodeposition process, the layers flowed rapidly to the edges of the crystal. Several growth centers were present on a surface and the growth layers originating from them grew together completely without discontinuities. As result of this, well-developed crystal plates with flat faces and sharp edges and corners, containing angles of 60° and 120° , are obtained [46]. The typical hexagonal crystal plates (the parts in the circles) recorded from the side of regular crystal formed at an overpotential of 20 mV are shown in Fig. 2.26a. On the basis of the analysis of Fig. 2.24 and the XRD analysis of Pb particles electrodeposited at 20 mV (Pb crystallites only oriented in the (111) plane), it is clear that these hexagonal crystal faces correspond to the (111) plane. The regular crystals are only constructed from them, and hence, they represent single crystals of the (111) orientation. Simultaneously, the powder obtained by tapping the deposit electrodeposited at an overpotential of 20 mV is a collection of Pb single crystals which is confirmed by the XRD analysis. Summary, Pb crystallites oriented in the (111) plane are formed at the low overpotential which indicates the affiliation of this plane to the group of slow-growing faces.

On the other hand, irregular crystals, needle-like and fern-like dendrites, are formed by the electrodeposition processes at the high overpotentials, and the both types of growth centers are responsible for their formation and growth. The growth layers of center type appear on the sides of the needle-like form because the current density and overpotential are lower on the sides than at the tip of a dendrite [46]. An inspection of a space lattice model showed that a morphological form may very well be bounded by only (111) faces, as shown in Fig. 2.26b for a side of one irregular crystal. In this way, the existence of the strong (111) preferred orientation

Fig. 2.26 The hexagonal growth layers formed at overpotentials of: (a) 20 mV and (b) 80 mV, and (c) a rounded tip of the irregular form electrodeposited at 80 mV (Reproduced from [62] by permission of The Royal Society of Chemistry.)



of powder particles primarily consisting of irregular crystals (precursors of dendrites) and dendrites is very clear (Figs. 2.21, 2.22, and 2.23). At the higher overpotentials, the growth layers flowed slowly and often stop before they have reached the edges of the crystal face [46]. New layers form which stop still earlier. The growth layers spread from many centers and they merge incompletely making rounded edges and corners, as shown in Fig. 2.26c for the tip of the dendrite “in the construction.” Hence, it is obvious that the origin of the crystallites oriented in the (200), (220), (311), and (331) planes is of growth centers at the edges and corners, and these planes can be denoted by fast-growing faces [65]. The larger the overpotential, the larger the ratio of the lead crystallites oriented in the (200), (220), (311), and (331) planes is obtained (Fig. 2.23).

Then, the strong (111) preferred orientation of lead deposits can be summarized as follows: overpotentials and current densities responsible for the crystal growth based on growth centers of “edge and corner type” are higher than those responsible for crystal growth based on growth centers of “center type.” It means that the current densities are higher at the tips of the growing forms than at their sides. In the growth process, slow-growing (111) face will survive constructing all elements of dendrites (both stalk and branches), and hence, causing the predominant orientation of Pb crystallites in this plane, as confirmed in Fig. 2.23. Simultaneously, the fast-growing (200), (220), (311) and (331) planes will disappear which explain considerably smaller the presence of Pb crystallites in these planes than in the (111) plane.

As already mentioned, the two groups of dendrites are formed by the electrodeposition at 140 mV: the needle-like and fern-like ones (Fig. 2.22). The needle-like dendrites grow along the cube face diagonal [110] of the FCC lattice [46]. The fern-like dendrites are constructed from the stalk and primary branches (primary (P) type) with an approximate angle of 60° between the stalk and the branches. Then, it is obvious that the dendrites branch along the face diagonals [110] of the unit cube which is the most favored from an energetic point of view [46]. Due to these characteristics, the fern-like lead dendrites are denoted 2D[110] 60° in Wranglen’s classification of a dendrite.

Also, the effect of the current density distribution [66] should be not excluded in the consideration of growth of dendrites because the current lines are primarily concentrated at the tips of these growing needle-like forms.

As already mentioned, morphology of lead dendrites strongly depended on the type of electrolyte (see Sect. 2.3.2.2). In Figs. 2.27 and 2.28 are shown the typical powder particles obtained by the tapping lead deposits electrodeposited at an overpotential of 100 mV from the nitrate ($0.10 \text{ M Pb(NO}_3)_2 + 2.0 \text{ M NaNO}_3$; Fig. 2.27) and the complex ($0.10 \text{ M Pb(CH}_3\text{COO)}_2 + 1.5 \text{ M NaCH}_3\text{COO} + 0.15 \text{ M CH}_3\text{COOH}$; Fig. 2.28) electrolytes.

From Figs. 2.27 and 2.28, it is very clear that there is no difference between the lead surface morphologies electrodeposited at the electrode surface (Figs. 2.17 and 2.18) and powder particles obtained after their removal from the electrode surface (Figs. 2.27 and 2.28, respectively) [43].

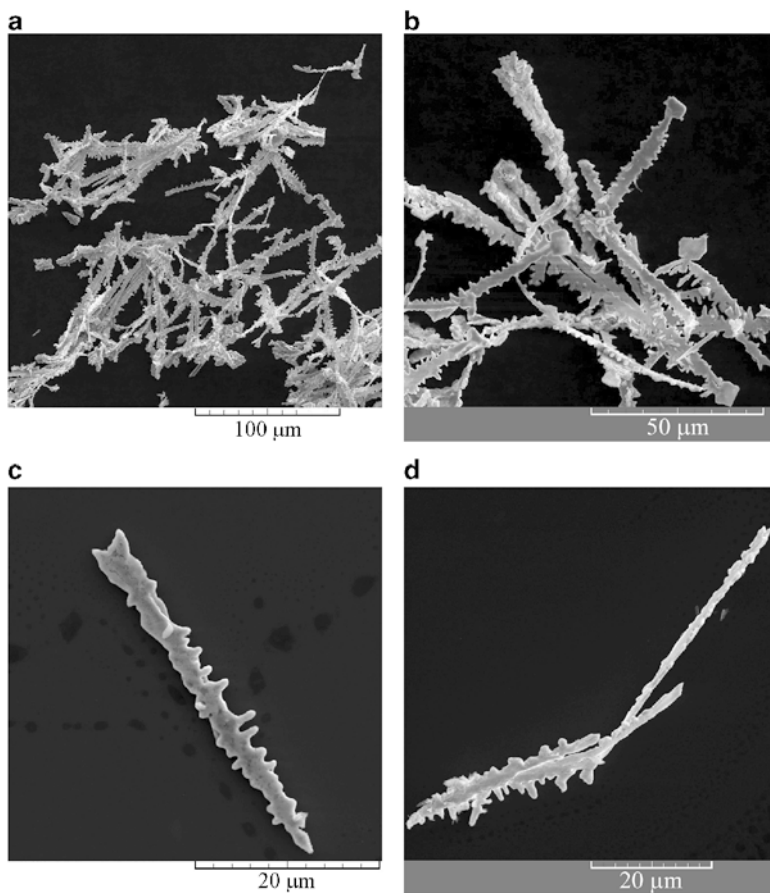


Fig. 2.27 Powder particles obtained by tapping the lead powdered deposit formed by electrodeposition at an overpotential of 100 mV from 0.10 M $\text{Pb}(\text{NO}_3)_2$ + 2.0 M NaNO_3 (Reprinted from [43] with permission from Elsevier and [65] with permission from Serbian Chemical Society.)

Powder particles shown in Figs. 2.27 and 2.28 are used for the XRD analysis, and the corresponding XRD patterns are shown in Fig. 2.29 [65]. It is very clear from Fig. 2.29 that the shown XRD patterns were very similar to each other. Pb crystallites were predominately oriented in the (111) plane. Aside from Pb crystallites oriented in this plane, the presence of crystallites oriented in the (200), (220), (311), and (331) planes was also observed. Anyway, unlike of the completely different morphology of powder particles, the crystallographic structure was practically the same in the both cases (the strong (111) preferred orientation).

The different shapes of Pb deposits, such as octahedral, nonregular crystals, zigzag nanowires, and nanoclusters, were synthesized by the electrodeposition from complex acetate electrolytes in the galvanostatic regime on the different substrates, like Cu, Ti, and Al [67]. The common characteristic of all these morphological

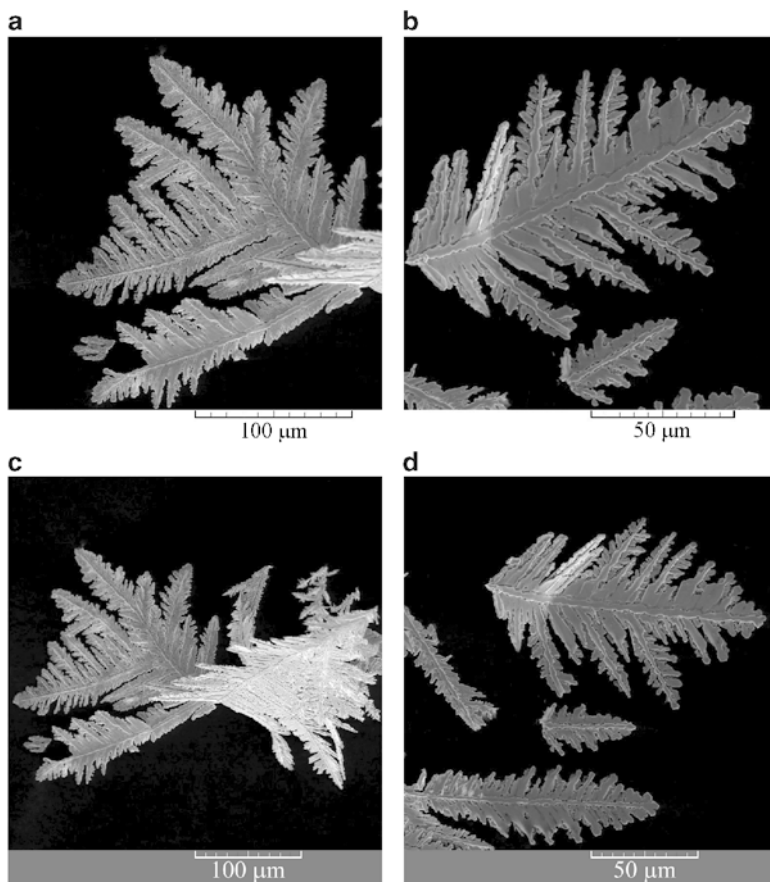


Fig. 2.28 Powder particles obtained by tapping the lead powdered deposit formed by electrodeposition at an overpotential of 100 mV from 0.10 M $\text{Pb}(\text{CH}_3\text{COO})_2$ + 1.5 M NaCH_3COO + 0.15 M CH_3COOH (Reprinted from [43] with permission from Elsevier and [65] with permission from Serbian Chemical Society.)

forms is the dominant orientation of Pb crystallites in the (111) plane. Electron diffraction (ED) study also confirmed a growth direction in single zigzag lead nanowire along the [1 1 0] axis [67].

It can be concluded from the hitherto consideration that the final morphology of electrodeposited metal (in this case, Pb) is determined by the current density or overpotential applied, composition of solution, the type of working electrode, temperature, etc., while the interior structure of these surface morphologies is only determined by the characteristics and nature of metal, and it does not depend on the electrodeposition conditions. In our case, morphologies of lead deposits were substantially different, but the strong (111) preferred orientation was always obtained.

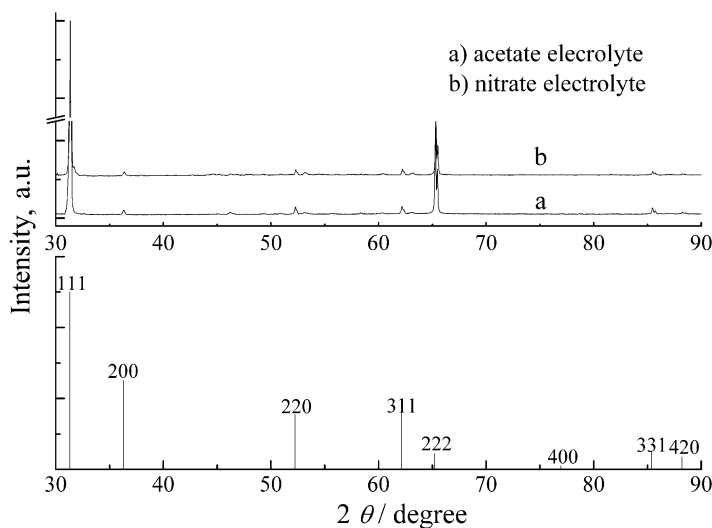


Fig. 2.29 The XRD patterns of the lead powder particles electrodeposited from electrolytes 0.10 M $\text{Pb}(\text{CH}_3\text{COO})_2$ + 1.5 M NaCH_3COO + 0.15 M CH_3COOH and 0.10 M $\text{Pb}(\text{NO}_3)_2$ + 2.0 M NaNO_3 (Reprinted from [65] with permission from Serbian Chemical Society.)

2.5 Electrodeposition of Pb from Alkaline Electrolytes

Unlike of most acid electrolytes which are toxic, alkaline electrolytes are more appropriate from the environmental standpoint [68]. Additionally, alkaline solutions are less corrosive to plants and equipment. The two most usual alkaline electrolytes used for the deposition of lead are the pyrophosphate and plumbite (based on hydroxide ions) processes. From alkaline electrolytes, a solution containing 0.10 M $\text{Pb}(\text{NO}_3)_2$ in 2.0 M NaOH is analyzed because it gives the highest rate of deposition which is very suitable for industrial purposes [8].

2.5.1 Polarization Characteristics

Polarization curve for lead electrodeposition from 0.10 M $\text{Pb}(\text{NO}_3)_2$ in 2.0 M NaOH is shown in Fig. 2.30. In relation to acid electrolytes (Fig. 2.13), the beginning of the lead electrodeposition process is shifted to the higher overpotential for about 5 mV indicating a sensitivity of the reaction of Pb electrodeposition on the type of electrolyte. Also, Pb electrodeposition reaction is sensitive to the substrate type. For example, Pb electrodeposition on SS316 stainless steel occurs at a slightly higher overpotential than at a platinum one [9]. Similar to the polarization curves for Pb electrodeposition from nitrate and acetate electrolytes, this polarization curve

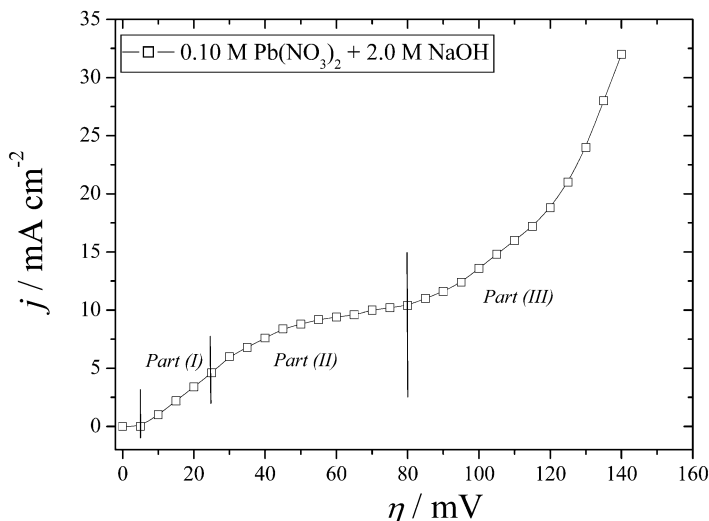


Fig. 2.30 The polarization curve for lead electrodeposition from 0.10 M $\text{Pb}(\text{NO}_3)_2$ + 2.0 M NaOH

consists of three parts: (a) the ohmic part—*Part (I)*; in the range of overpotentials between 5 and 25 mV, (b) the diffusion part—*Part (II)*; in the range of overpotentials between 25 and 80 mV, and (c) the part characterized by the fast increase of the current with increasing the overpotential after the inflection point ($\eta = 80$ mV)—*Part (III)* [69]. The plateau of the limiting diffusion current density determined in a way described in Sect. 2.3.2.1 was between 39.5 and 80 mV.

2.5.2 Morphological and Crystallographic Analysis of Pb Powdered Deposits

Morphologies of lead deposits obtained by electrodeposition in the potentiostatic mode at overpotentials corresponding to different positions at the polarization curve are shown in Figs. 2.31, 2.32, 2.33, and 2.34.

In Fig. 2.31 are shown the regular crystals obtained in the ohmic control at an overpotential of 20 mV. As expected, the fern-like dendrites were dominant morphological forms obtained during the diffusion controlled electrodeposition. The typical dendrites obtained at an overpotential of 50 mV are shown in Fig. 2.32. Aside from the dendrites, the small irregular crystals (precursors of dendrites) were formed by the electrodeposition at 50 mV (part in the circle in Fig. 2.32a). The more branchy dendrites and the considerably larger their number was formed during electrodeposition at an overpotential of 80 mV, which corresponds to the end of the

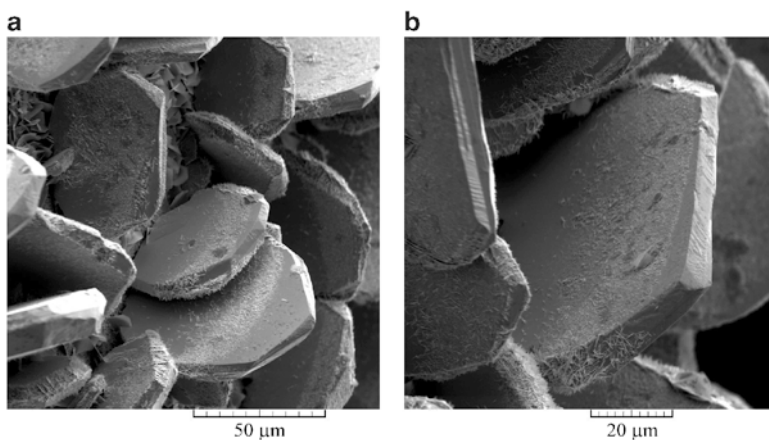


Fig. 2.31 Morphologies of electrodeposited lead obtained in the ohmic controlled electrodeposition at $\eta = 20$ mV from 0.10 M $\text{Pb}(\text{NO}_3)_2 + 2.0$ M NaOH

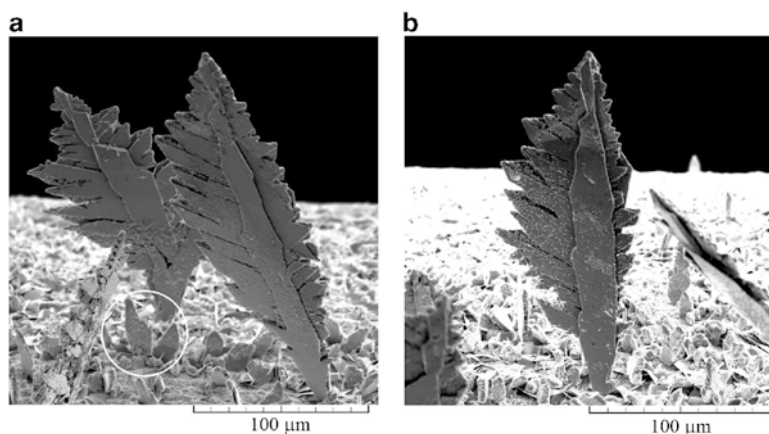


Fig. 2.32 Morphologies of electrodeposited lead obtained at the plateau of the limiting diffusion current density ($\eta = 50$ mV) from 0.10 M $\text{Pb}(\text{NO}_3)_2 + 2.0$ M NaOH

plateau of the limiting diffusion current density (Fig. 2.33). It is necessary to note that the dendrites were only morphological forms formed during the electrodeposition at this overpotential. The very branchy dendrites, as the only type of the surface morphology, were also obtained at 100 mV (Fig. 2.34) in the zone of the fast growth of the current density with the overpotential.

From Fig. 2.32, it can be clearly seen that the primary (P) type of a dendrite is formed at 50 mV. Increasing overpotential causes branching of dendrites, and the mixture of primary (P) and secondary (S) dendrites was predominately formed at 80 mV (Fig. 2.33). Finally, the dendrites of S type are

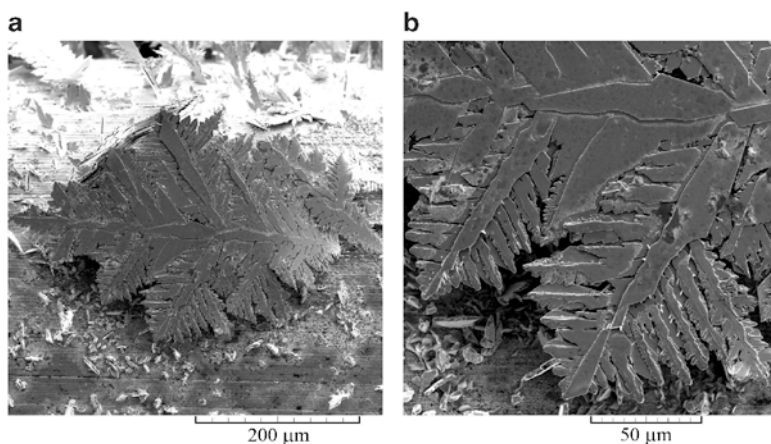


Fig. 2.33 Morphologies of electrodeposited lead obtained at the end of the plateau of the limiting diffusion current density ($\eta = 80$ mV) from 0.10 M $\text{Pb}(\text{NO}_3)_2 + 2.0$ M NaOH

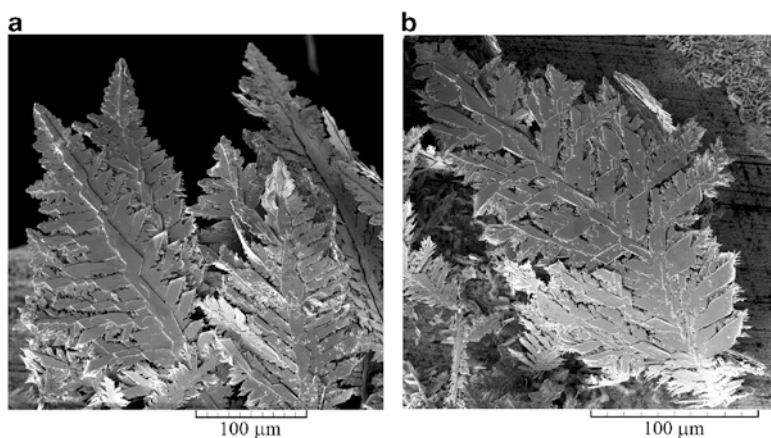
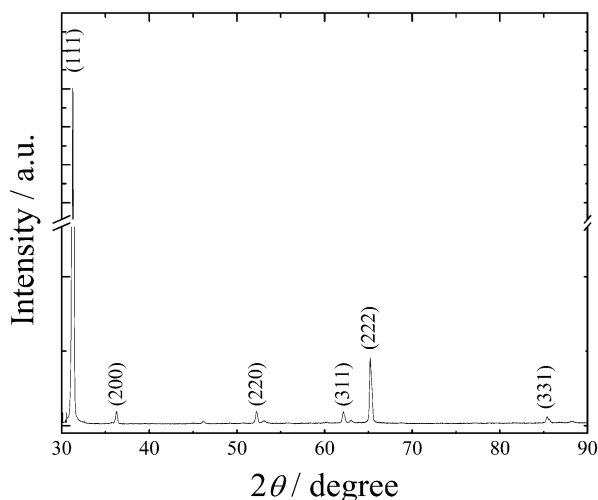


Fig. 2.34 Morphologies of electrodeposited lead obtained in the zone of the fast growth of the current density with the overpotential ($\eta = 100$ mV) from 0.10 M $\text{Pb}(\text{NO}_3)_2 + 2.0$ M NaOH

predominately formed at 100 mV (Fig. 2.34). Although the (P) and (S) dendrites are the dominant shapes of dendrites formed from this electrolyte, the presence of the tertiary branches developed from some secondary branches is also visible (Fig. 2.33b; the enlarged detail from Fig. 2.33a). The two-dimensional (2D) shape of the fern-like dendrites is clearly visible from Figs. 2.32, 2.33, and 2.34.

It is necessary to note that the shape of regular (single) crystals did not depend on the type of electrolyte. Contrary, the surface morphology of dendrites strongly depended on the type of electrolyte; the dendrites electrodeposited from this

Fig. 2.35 The XRD pattern of the powder particles obtained by the tapping lead deposit electrodeposited at an overpotential of 100 mV from 0.10 M Pb (NO_3)₂ + 2.0 M NaOH



alkaline electrolyte are more similar to those obtained from the acetate electrolyte than those obtained from the nitrate ones.

The crystallographic characteristics of Pb crystals were examined by the XRD analysis of powder particles obtained by tapping the lead deposit electrodeposited at an overpotential of 100 mV, and the corresponding XRD pattern is shown in Fig. 2.35. Lead crystallites were predominately oriented in the (111) plane. The ratio of crystallites oriented in the (200), (220), (311), and (331) planes was considerably smaller than those oriented in the (111) plane. The size of crystallites is determined by Williamson–Hall method and was estimated to be 36.5 nm. The quantitative analysis of this Pb powder showed its 100 % purity indicating the significance of the electrolysis processes in the production of powdered forms of high purity.

It is confirmed that the crystallographic (interior) structure of Pb crystals is determined by the nature of lead, and it is not associated with the type of used electrolyte, and hence, with the surface morphology.

2.5.3 Final Discussion of the Presented Results

The crystallographic aspects of formation of powder particles cannot be analyzed separately than electrochemical ones. Schematic diagram illustrating the overpotential dependent formation and growth of fern-like dendrites is given in Fig. 2.36. At the low overpotential (I. in Fig. 2.36), current lines are equally distributed, and regular crystals like those shown in Fig. 2.31 are formed. Crystal growth based only on the growth centers present in the interior of the crystal faces is responsible for formation of the regular crystals, which is confirmed by the XRD

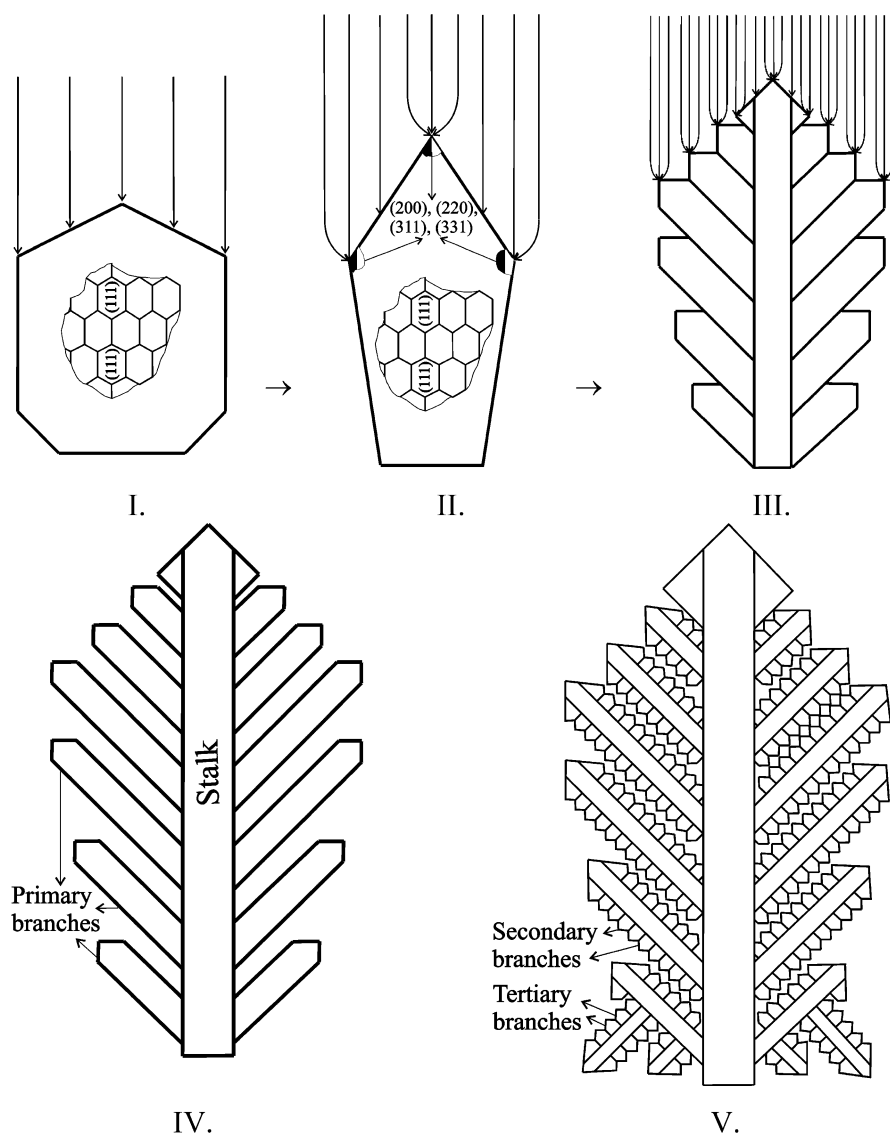


Fig. 2.36 Schematic diagram illustrating the overpotential dependent growth of fern-like dendrites

analysis of this surface morphology type. As already mentioned, these regular crystals represent of single crystals of the (111) orientation [62]. Increasing overpotential leads to a concentration of current lines in the first place at the tips and corners of growing forms causing faster growth on them than at the sides of crystals and in the vicinity of the electrode surface (the current density distribution

Table 2.1 The ranges of overpotentials belonging to the ohmic and diffusion parts of the polarization curves, as well as the length of the plateaus of the limiting diffusion current density for the given electrolytes

Solution for lead electrodeposition	The ohmic part of the polarization curve (mV)	The diffusion part of the polarization curve (mV)	The plateau of the limiting diffusion current density (mV)
0.10 M $\text{Pb}(\text{NO}_3)_2$ + 2.0 M NaNO_3	0–15	15–55	28.5–55
0.10 M $\text{Pb}(\text{CH}_3\text{COO})_2$ + 1.5 M NaCH_3COO + 0.15 M CH_3COOH	0–20	20–70	33–70
0.10 M $\text{Pb}(\text{NO}_3)_2$ + 2.0 M NaOH	5–25	25–80	39.5–80

effect) [66]. Hence, the current densities are higher at the tips and corners of the growing forms (the growth based on edge and corner growth centers) than at their sides (the growth based on growth centers of the center type). As a result of this, irregular crystals or precursors of dendrites are formed (II. in Fig. 2.36). The origin of Pb crystallites oriented in the (200), (220), (311), and (331) planes is just of crystal growth on the tips and corners of growing crystals. Simultaneously, the sides of the crystals are constructed from Pb crystallites oriented in the (111) plane [62]. The typical irregular crystals (precursors of dendrites) obtained from this alkaline electrolyte are shown in the circle in Fig. 2.32a. The current density, and hence, concentration of current lines at the growing crystals increases with increasing the overpotential leading to the appearance of dendrites at the higher overpotentials (III. in Fig. 2.36). Please note that for reasons of simplification, the only one part of current lines is illustrated in Fig. 2.36. During the growth of dendrites, the current densities increase exponentially. The larger the applied overpotential, the faster exponential increase during electrodeposition is observed [30]. Due to the increase of the number of growth centers at which a concentration of current lines takes place, branching of dendrites is observed resulting in the development of primary, secondary, and tertiary branches in them (IV. and V. in Fig. 2.36 and Figs. 2.32, 2.33, and 2.34).

For the alkaline electrolyte containing 0.10 M $\text{Pb}(\text{NO}_3)_2$ in 2.0 M NaOH , both ohmic and diffusion parts at the polarization curve were shifted to higher overpotentials in relation to those observed for the acid electrolytes based on nitrate and acetate ions (for the same concentration of 0.10 M $\text{Pb}(\text{II})$ ions). In Table 2.1 are given the ranges of overpotentials belonging to the ohmic and diffusion control, as well as the lengths of the plateau of the limiting diffusion current density for the nitrate, acetate, and alkaline electrolytes. The increasing trend in row nitrate < acetate < hydroxide ions is clearly visible from Table 2.1.

From the morphological point of view, morphologies of Pb dendrites (Figs. 2.32, 2.33, and 2.34) are more similar to those obtained from the acetate than from the nitrate electrolytes. The ramified dendrites belonging to the secondary (S) type are formed from both acetate and alkaline electrolytes. Unlike of this type of a dendrite,

the needle-like and primary (P) dendrites were only formed from the nitrate electrolyte [30, 32, 43, 62, 65].

The common characteristic of the acetate and alkaline electrolytes is their affiliation to the group of complex electrolytes. In the case of the acetate electrolyte, the increase of the plateau of the limiting diffusion current density and ramification of dendrites in relation to the nitrate electrolyte was ascribed to the process of the complex formation of Pb(II) ions with the acetate ions [43]. One of the consequences of the process of complex formation was a lowering of the exchange current density, j_0 , for electrodeposition process, and hence, the decrease of a rate of electrochemical process. For the alkaline electrolytes based on hydroxide ions, the reduction of lead occurs entirely through the complex species and not through Pb(II) ions [8]. Lead makes different complexes with hydroxide ions, such as $[\text{PbOH}]^+$, $[\text{Pb}(\text{OH})_2]$, $[\text{Pb}(\text{OH})_3]^-$, $[\text{Pb}_2(\text{OH})]^{3+}$, $[\text{Pb}_3(\text{OH})_4]^{2+}$, $[\text{Pb}_4(\text{OH})_4]^{4+}$, and $[\text{Pb}_6(\text{OH})_8]^{4+}$ [70, 71]. In the very alkaline electrolyte solution, pH over 12 (as in this case), $[\text{Pb}(\text{OH})_3]^-$ complex becomes a major species in the solution [72–74], and probably the reduction of lead occurs entirely through this complex.

Hence, as a result of the processes of the complex formation, the increase of both the plateau of the limiting diffusion current density and ramification of dendrites is observed. It is very clear that this is very good auxiliary diagnostic criteria for the comparison of electrodeposition systems characterized by the large exchange current density ($j_0 \rightarrow \infty$) with point of view of the different j_0 values (i.e., rate of electrochemical process) for which there is no precise and reference method for the determination of j_0 values.

The degree of the change of the both polarization and morphological characteristics can be correlated with the stability of formed complexes. Namely, Pb(II) ions form relatively weak complexes with acetate ions. The stability constants for the acetate complexes are $\log K_1 = 2.33$ and $\log \beta_2 = 3.60$. On the other hand, Pb makes stronger complex with hydroxide ions than with the acetate ions. For example, the stability constant of $[\text{Pb}(\text{OH})_3]^-$ complex, which is primary species in very alkaline solutions (2 M NaOH), is $\log \beta_3 = 13.3$ [70, 74]. This constant is about 5×10^9 times larger than the constant for the acetate complex. Anyway, the stronger complex is formed, the stronger effect on the polarization characteristics and surface morphology of electrodeposited metal is observed. In this case, this is manifested through the increase of the plateau of the limiting diffusion current density and formation of larger number of dendrites of S type, as well as by the appearance of tertiary branches in the dendrites of S type from the alkaline electrolyte in relation to the acetate one.

2.6 Conclusions

A detailed mechanism of lead electrodeposition is presented in this chapter. Unlike of long-time belief that electrodeposition of metals characterized by high exchange current densities is the diffusion controlled process in the whole range of

overpotentials, it is shown that lead electrodeposition occurs in the conditions of the mixed ohmic-diffusion, or even, the full ohmic control. With the increasing concentration of Pb(II) ions in the solution, the ratio of the ohmic control to the total control of electrodeposition process increased. At the higher concentrations of Pb(II) ions, the electrodeposition process became completely ohmic controlled.

The polarization characteristics of lead were correlated with morphology of electrodeposited lead. The regular crystals were obtained in the ohmic control. The XRD analysis showed that they represent single crystals of the (111) preferred orientation. The shape of single crystals did not depend on the type of used electrolyte.

The shape of dendrites formed in the diffusion control strongly depends on the type of electrolyte. Dendrites formed from the complex electrolytes (acetate and alkaline ones) are more branchy than those obtained from the basic (nitrate) electrolyte. The dendrites obtained from the basic electrolyte largely belonged to the primary (P) type. Contrary, dendrites obtained from the complex electrolytes were of the secondary (S) type. Unlike of the strong effect of the type of electrolyte on morphology of dendrites, all dendritic forms were predominately oriented in the (111) plane.

For all examined electrolytes, the fast increase of the current density with increasing the overpotential after the inflection point was ascribed to the activation control at the tips of formed dendrites.

Also, the polarization characteristics and the morphology of lead electrodeposited from the complex electrolytes were correlated with the stability constant of lead complex.

Acknowledgments The authors are grateful to Dr. Goran Branković for SEM analysis of investigated systems, to Dr. Vesna Maksimović for the XRD analysis of the powder particles, as well as to Prof. Dr. Predrag Živković for the digital simulations.

The work was supported by the Ministry of Education, Science and Technological Development of the Republic of Serbia under the research project: "Electrochemical synthesis and characterization of nanostructured functional materials for application in new technologies" (No. 172046).

References

1. Pavlov D (1993) *J Power Sources* 42:345
2. Rashkova B, Guel B, Potzschke RT, Staikov G, Lorenz WJ (1998) *Electrochim Acta* 43:3021
3. Ehlers C, König U, Staikov G, Schultze JW (2002) *Electrochim Acta* 47:379
4. Avellaneda CO, Napolitano MA, Kaibara EK, Bulhoes LOS (2005) *Electrochim Acta* 50:1317
5. <http://www.nuclead.com/leadpowderapps.html>.
6. Cherevko S, Xing X, Chung C-H (2011) *Appl Surf Sci* 257:8054
7. Winand R (1994) *Electrochim Acta* 39:1091
8. Carlos IA, Malaquias MA, Oizumi MM, Matsuo TT (2001) *J Power Sources* 92:56
9. Wong SM, Abrantes LM (2005) *Electrochim Acta* 51:619
10. Doulakas L, Novy K, Stucki S, Comninellis Ch (2000) *Electrochim Acta* 46:349

11. Scharifker B, Hills G (1983) *Electrochim Acta* 28:879
12. Mostany J, Parra J, Scharifker BR (1986) *J Appl Electrochem* 16:333
13. Mostany J, Mozota J, Scharifker BR (1984) *J Electroanal Chem* 177:25
14. Popov KI, Krstajić NV, Pantelić RM, Popov SR (1985) *Surf Technol* 26:177
15. Exposito E, Gonzalez-Garcia J, Bonete P, Montiel V, Aldaz A (2000) *J Power Sources* 87:137
16. Popov KI, Stojilković ER, Radmilović V, Pavlović MG (1997) *Powder Technol* 93:55
17. Ghergari L, Oniciu L, Muresan L, Pantea A, Topan VA, Ghertoiu D (1991) *J Electroanal Chem* 313:303
18. Muresan L, Oniciu L, Froment M, Maurin G (1992) *Electrochim Acta* 37:2249
19. Muresan L, Oniciu L, Wiart R (1993) *J Appl Electrochem* 23:66
20. Muresan L, Oniciu L, Wiart R (1994) *J Appl Electrochem* 24:332
21. Hazza A, Pletcher D, Wills R (2004) *Phys Chem Chem Phys* 6:1773
22. Pletcher D, Wills R (2004) *Phys Chem Chem Phys* 6:1779
23. Ghali E, Girgis M (1985) *Metall Mater Trans B* 16:489
24. Carlos IA, Siqueira JLP, Finazzi GA, de Almeida MRH (2003) *J Power Sources* 117:179
25. Popov KI, Živković PM, Grgur BN (2007) *Electrochim Acta* 52:4696
26. Popov KI, Živković PM, Krstić SB, Nikolić ND (2009) *Electrochim Acta* 54:2924
27. Popov KI, Živković PM, Nikolić ND (2010) The effect of morphology of activated electrodes on their electrochemical activity. In: Djokić SS (ed) *Electrodeposition: Theory and Practice, Modern Aspects of Electrochemistry*, vol 48. Springer, pp 163–213
28. Popov KI, Nikolić ND (2012) General Theory of Disperse Metal Electrodeposits Formation. In: Djokić SS (ed) *Electrochemical Production of Metal Powders, Modern Aspects of Electrochemistry*, vol. 54. Springer, pp 1–62
29. Popov KI, Nikolić ND, Živković PM, Branković G (2010) *Electrochim Acta* 55:1919
30. Nikolić ND, Branković G, Lačnjevac U (2012) *J Solid State Electrochem* 16:2121
31. Jović VD, Nikolić ND, Lačnjevac UČ, Jović BM, Popov KI (2012) Morphology of Different Electrodeposited Pure Metal Powders. In: Djokić SS (ed) *Electrochemical Production of Metal Powders, Modern Aspects of Electrochemistry*, Vol. 54. Springer, pp 63–123
32. Nikolić ND, Popov KI, Živković PM, Branković G (2013) *J Electroanal Chem* 691:66
33. Levich VG (1962) *Physicochemical Hydrodynamics*. Prentice – Hall, Inc: Englewood Cliffs, Ch. 2, NJ
34. Blagojević NS, Maksimović MD, Popov KI (1978) *Chem Eng J* 16:35
35. Lorenz W (1954) *Z Electrochem* 58:912 (in German)
36. Mattsson BE, Bockris JO'M (1959) *Trans Faraday Soc* 55:1586
37. Newman JS (1973) *Electrochemical Systems*. Prentice-Hall, Inc. Englewood Cliffs, N. J.
38. Fetter K (1967) *Electrochemical Kinetics*. Moscow, Khimiya, (in Russian)
39. Nikolić ND, Popov KI, Pavlović LJ, Pavlović MG (2007) *Sensors* 7:1
40. Djokić SS, Nikolić ND, Živković PM, Popov KI, Djokić NS (2011) *ECS Trans* 33:7
41. Mandke MV, Han S-H, Pathan HM (2012) *CrystEngComm* 14:86
42. Ni Y, Zhang Y, Zhang L, Hong J (2011) *CrystEngComm* 13:794
43. Nikolić ND, Vaštag DjDj, Živković PM, Jokić B, Branković G (2013) *Adv Powder Technol* 24:674
44. Popov KI, Krstajić NV, Čekerevac MI (1996) The mechanism of formation of coarse and disperse electrodeposits. In: White RE, Conway BE, Bockris JO'M (eds) *Modern Aspects of Electrochemistry*, vol 30. Plenum Press, New York, pp 261–312
45. Popov KI, Pavlović MG, Jovičević JN (1989) *Hydrometallurgy* 23:127
46. Wranglen G (1960) *Electrochim Acta* 2:130
47. Popov KI, Djokić SS, Grgur BN (2002) *Fundamental aspects of electrometallurgy*. Kluwer Academic/Plenum Publishers, New York
48. Despić AR, Popov KI (1972) Transport controlled deposition and dissolution of metals. In: Conway BE, Bockris JO'M (eds) *Modern Aspects of Electrochemistry*, vol 7. Plenum Press, New York, pp 199–313

49. Diggle JW, Despić AR, Bockris JO'M (1969) The mechanism of the dendritic electrocrystallization of zinc. *J Electrochem Soc* 116:1503
50. Nikolić ND, Popov KI, Pavlović LjJ, Pavlović MG (2006) *J Electroanal Chem* 588:88
51. Nikolić ND, Pavlović LjJ, Pavlović MG, Popov KI (2008) *Powder Technol* 185:195
52. Nikolić ND, Popov KI (2010) Hydrogen co-deposition effects on the structure of electrodeposited copper. In: Djokić SS (ed) *Electrodeposition: Theory and Practice, Modern Aspects of Electrochemistry*, vol 48. Springer, pp 1–70
53. Nikolić ND (2012) Porous Copper Electrodes Formed by the Constant and the Periodically Changing Regimes of Electrolysis. In: Djokić SS (ed) *Electrochemical Production of Metal Powders, Modern Aspects of Electrochemistry*, Vol. 54, Springer, pp 187–249
54. Nikolić ND, Branković G, Pavlović MG (2012) *Powder Technol* 22:271
55. Orhan G, Hapci G (2010) *Powder Technol* 201:57
56. Orhan G, Gezgin GG (2012) *J Serb Chem Soc* 77:651
57. Živković PM, Nikolić ND, Gvozdenović M, Popov KI (2009) *J Serb Chem Soc* 74:291
58. Popov KI, Krstajić NV, Popov SR (1983) *Surf Technol* 20:203
59. Nikolić ND, Popov KI (2012) Electrodeposition of Copper Powders and Their Properties. In: Djokić SS (ed) *Electrochemical Production of Metal Powders, Modern Aspects of Electrochemistry*, Vol. 54, Springer, pp 125–185
60. Nikolić ND, Pavlović LjJ, Krstić SB, Pavlović MG, Popov KI (2008) *Chem Eng Sci* 63:2824
61. Popov KI, Grgur BN, Stojilković ER, Pavlović MG, Nikolić ND (1997) *J Serb Chem Soc* 62:433
62. Nikolić ND, Maksimović VM, Branković G, (2013) *RSC Adv* 3:7466
63. Milchev A (2002) *Electrocrystallization, Fundamentals of Nucleation and Growth*. Kluwer Academic Publishers, Boston/Dordrecht/London, p. 24
64. Bockris JO'M, Reddy AKN, Gamboa-Aldeco M (2000) *Modern Electrochemistry 2A, Fundamentals of Electrodics*, Kluwer Academic / Plenum Publishers, New York, p. 1333
65. Nikolić ND, Maksimović VM, Branković G, Živković PM, Pavlović MG (2013) *J Serb Chem Soc* 78:1387
66. Popov KI, Živković PM, Nikolić ND (2011) *J Serb Chem Soc* 76:805
67. Yao C-Z, Liu M, Zhang P, He X-H, Li G-R, Zhao W-X, Liu P, Tong Y-X (2008) *Electrochim Acta* 54:247
68. Jordan M (2010) Electrodeposition of lead and lead alloys, in: M. Schlesinger, M. Paunovic (Eds.), *Modern Electroplating*, Fifth Edition, John Wiley & Sons, Inc., p. 251
69. Nikolić ND, Vaštag DjDj, Maksimović VM, Branković G, *Trans Nonferrous Met Soc China*, in press
70. NIST Standard Reference Database 46, NIST Critically Selected Stability Constants of Metal Complexes Database, version 3.0, compiled by R.M. Smith and A.E. Martell, U.S. Department of Commerce, National Institute of Standards and Technology, Gaithersburg, MD 20899, USA
71. Kratgen J (1978) *Atlas of Metal-Ligand Equilibria in Aqueous Solution*. Series in Analytical Chemistry, Ellis Horwood, Chichester. UK
72. Cukrowska E, Cukrowski I (1998) *Talanta* 47:1175
73. Pereira M, Mantas PQ (1998) *J Eur Ceram Soc* 18:565
74. Wang Y, Chai L, Chang H, Peng X, Shu Y (2009) *Trans Nonferrous Met Soc China* 19:458.

Electrodeposition and Surface Finishing

Fundamentals and Applications

Djokić, S.S. (Ed.)

2014, XIV, 363 p. 270 illus., 25 illus. in color., Hardcover

ISBN: 978-1-4939-0288-0